NASA TECHNICAL MEMORANDUM

NASA TM X-2184

NASA TM X-2184

# EXPERIMENTAL INVESTIGATION OF THE INTERACTION OF A NACELLE-MOUNTED SUPERSONIC PROPULSION SYSTEM WITH A WING BOUNDARY LAYER

*by Glenn A. Mitchell and David F. Johnson*

*Lewis Research Center*
*Cleveland, Ohio 44135*

NATIONAL AERONAUTICS AND SPACE ADMINISTRATION • WASHINGTON, D. C. • MARCH 1971

| 1. Report No. | 2. Government Accession No. | 3. Recipient's Catalog No. |
|---|---|---|
| NASA TM X-2184 | | |

| 4. Title and Subtitle | 5. Report Date |
|---|---|
| EXPERIMENTAL INVESTIGATION OF THE INTERACTION OF A NACELLE-MOUNTED SUPERSONIC PROPULSION SYSTEM WITH A WING BOUNDARY LAYER | March 1971 |
| | 6. Performing Organization Code |
| 7. Author(s) | 8. Performing Organization Report No. |
| Glenn A. Mitchell and David F. Johnson | E-5983 |
| | 10. Work Unit No. |
| 9. Performing Organization Name and Address | 720-03 |
| Lewis Research Center<br>National Aeronautics and Space Administration<br>Cleveland, Ohio 44135 | 11. Contract or Grant No. |
| | 13. Type of Report and Period Covered |
| 12. Sponsoring Agency Name and Address | Technical Memorandum |
| National Aeronautics and Space Administration<br>Washington, D.C. 20546 | 14. Sponsoring Agency Code |

15. Supplementary Notes

16. Abstract

A Mach 2.5 inlet nacelle was mounted adjacent to a simulated wing boundary layer. The extent of inlet-shock and boundary-layer interactions was determined for steady-state inlet operation and unstart transients. Transients were initiated with bypass closure and throat overcontraction for an inlet coldpipe combination, the inlet with a choke point at the compressor face station, and the inlet mated to a J85-GE-13 turbojet engine. Engine stalls were also used to initiate transients. The effects of boundary-layer height and wing-to-cowl-lip spacing were determined. The most severe transients were those resulting from engine stalls which produced wing-boundary-layer separations extending 2.8 cowl-lip diameters forward of the lip.

17. Key Words (Suggested by Author(s))

Inlet-shock and boundary-layer interaction
Unstart transients
Engine stall transients

18. Distribution Statement

Unclassified - unlimited

| 19. Security Classif. (of this report) | 20. Security Classif. (of this page) | 21. No. of Pages | 22. Price* |
|---|---|---|---|
| Unclassified | Unclassified | 43 | $3.00 |

*For sale by the National Technical Information Service, Springfield, Virginia 22151

# EXPERIMENTAL INVESTIGATION OF THE INTERACTION OF A NACELLE-MOUNTED SUPERSONIC PROPULSION SYSTEM WITH A WING BOUNDARY LAYER

by Glenn A. Mitchell and David F. Johnson

Lewis Research Center

## SUMMARY

A Mach 2.5 inlet was nacelle mounted adjacent to a simulated wing to determine the extent of inlet-shock and boundary-layer interaction resulting from steady-state inlet operation and unstart transients. Unstart transients were initiated with bypass closure and throat overcontraction for an inlet coldpipe combination, an inlet with a choke point at the compressor face station, and an inlet mated to a J85-GE-13 turbojet engine. Engine stalls were also used to initiate unstarts. The effects of boundary-layer height and wing-to-cowl-lip spacing were determined. The test was conducted in the Lewis 10- by 10-Foot Supersonic Wind Tunnel over a Mach number range from 2.3 to 2.7.

The most severe transients were the inlet unstarts following engine stall, which resulted in transient wing-boundary-layer separations extending 2.8 cowl-lip diameters forward of the cowl. The lateral extent of these separations would require an adjacent nacelle spacing of 4 cowl-lip diameters to avoid mutual interference. Unstarts resulting from bypass closure caused engine stall but produced smaller separation distances about 1.5 diameters forward of the cowl lip. The magnitude of the transient wing-boundary-layer separations following engine stall correlated with the engine mass-flow ratio at the initiation of stall when either stall caused unstart or stall followed unstart. In either case the hammershock required 12 to 13 milliseconds from the start of the transient to emerge from the inlet. The hammershock overpressures at the compressor face which resulted from compressor stall correlated with the absolute mass flow.

When unstarts were initiated without an engine installed, the extent of the boundary-layer separation was similar to that obtained with an engine if the inlet unstarted prior to compressor stall. It varied somewhat with the inlet internal volume forward of the choke point. The maximum wing pressure recorded during any transient was about 10 times the wing-flow-field static pressure. Increasing the wing-to-cowl-lip spacing or decreasing the boundary-layer thickness reduced the extent of the inlet-shock and boundary-layer interaction. Started inlet performance and the inlet restart cycle were not affected by moving the cowl lip inward to the edge of the wing boundary layer.

## INTRODUCTION

In a supersonic-cruise aircraft it may be desirable to put the engines in nacelles located underneath and close to the aircraft wing. This installation might provide favorable interference between the nacelle and wing flow fields and it shields the inlet to minimize angle-of-attack effects. However, the inlet is then located near the wing boundary layer. The interaction between the inlet system and this boundary layer determines the minimum distance between the inlet and wing and the minimum spacing which is required between adjacent nacelles for no mutual interference. Three regimes of interaction are evident: (1) Steady-state inlet operation at off-design Mach numbers produces a shock which may interact with the wing boundary layer and degrade inlet performance; (2) the shock structure produced by an unstarted inlet may produce a boundary-layer separation sufficiently large to interfere with the normal inlet restart cycle; (3) the maximum transient extent of the wing-boundary-layer separation, resulting from an inlet unstart, may cause the adjacent inlet to unstart.

These phenomena were studied in an experimental test program conducted in the Lewis 10- by 10-Foot Supersonic Wind Tunnel. A 15-foot (4.6-m) length of flat plate with boundary-layer generators (as used in ref. 1) provided a simulated wing boundary layer. The inlet was an axisymmetric Mach 2.5 design with 60 percent of the supersonic area contraction occurring internally. A complete discussion of the aerodynamic design of the inlet is present in reference 2. The inlet was installed in a nacelle which was mounted beneath the plate so as to place the cowl lip at the edge of the boundary layer. The extent of the wing-boundary-layer separation resulting from the inlet unstart transients was measured and analyzed for three inlet diffuser terminations: a long coldpipe, a choke point at the compressor face station, and a J85-GE-13 turbojet engine. Unstarts were initiated either by compressor stall, bypass closure, or throat overcontraction. The transient and steady-state interactions between the engine and inlet are reported in references 3 and 4 and the dynamic response of the inlet with each of the three diffuser terminations is reported in reference 5.

The effects of varying the distance of the inlet cowl lip from the edge of the wing boundary layer were determined for both steady-state and unstart transient conditions using the inlet and long coldpipe combination. The boundary-layer thickness was also varied. The test was conducted over a Mach number range from 2.3 to 2.7 at a Reynolds number of $3.88 \times 10^6$ based on cowl-lip diameter.

## SYMBOLS

A flow area, $ft^2$ ($m^2$)

| | |
|---|---|
| $A_c$ | capture area, $ft^2$ ($m^2$) |
| $A_{cowl}$ | flow area at cowl-lip station bounded by the model geometry, $ft^2$ ($m^2$) |
| $A_{min}$ | minimum internal flow area bounded by the model geometry, $ft^2$ ($m^2$) |
| $D_c$ | cowl-lip diameter, 18.63 in. (0.4732 m) |
| h | distance from plate surface, ft (m) |
| M | Mach number |
| $M_{cowl}$ | average cowl-lip-station Mach number |
| m | mass flow, lb/sec (kg/sec) |
| $m/m_w$ | mass-flow ratio for inlet in wing flow field |
| $m/m_0$ | mass-flow ratio for inlet in free stream |
| N | engine speed, rpm |
| $N^*$ | design engine speed, 16 500 rpm |
| P | total pressure, $lb/ft^2$ ($N/m^2$) |
| p | static pressure, $lb/ft^2$ ($N/m^2$) |
| T | total temperature, $^oR$ (K) |
| u | flow velocity, ft/sec (m/sec) |
| $W_{corr}$ | engine corrected airflow, lb/sec (kg/sec) |
| x | distance forward of inlet cowl-lip station, ft (m) |
| $x_t$ | distance forward of inlet cowl-lip station observed during unstart transient, ft (m) |
| y | lateral distance from inlet centerline, ft (m) |
| $\delta$ | boundary-layer height, ft (m) |
| $\theta$ | $T/518.7^o$ R (T/288.2 K) |

Subscripts:

| | |
|---|---|
| max | maximum |
| min | minimum |
| w | wing flow field |
| 0 | free-stream conditions |
| 1 | inlet-throat station |
| 2 | compressor-face station |

3 compressor-exit station

Superscript:

$\bar{}$ average

## APPARATUS AND PROCEDURE

### Model Details

A cross section of the Mach 2.5 axisymmetric mixed-compression inlet used in this test is presented in figure 1. The centerbody was translated to start the inlet and provide for off-design operation. At design Mach number, 40 percent of the supersonic flow area contraction was external and 60 percent was internal. External compression was performed with a $12.5^{\circ}$ half-angle conical centerbody. Internal compression was accomplished with the oblique shock generated by the $0^{\circ}$ cowl lip and the two reflected oblique shocks plus isentropic compression between these reflected shocks. The subsonic diffuser consisted of an initial throat region four hydraulic radii in length with a $1^{\circ}$ equivalent conical expansion followed by the main diffuser having an $8^{\circ}$ equivalent conical expansion. Additional details can be found in reference 2.

The inlet configuration is identical to configuration IIND' of reference 6. The performance of this configuration as reported in reference 6 is shown in figure 2. Vortex generators were installed on the centerbody in the subsonic diffuser to prevent centerbody flow separation in the bypass region during discharge of large overboard bypass flows. Performance bleed, which was provided by porous regions on the centerbody and cowl, was located both in the supersonic diffuser and in the throat region of the inlet. The total airflow removed by this bleed was about 5.5 percent of the capture mass flow. About 3.0 percent of the capture mass flow was bled through the secondary bypass and was used for engine cooling. The overboard bypass was used to match the inlet and engine airflows during normal operation with the inlet started. Step commands to this fast-acting bypass system were used to produce inlet unstarts during the test. Dynamic characteristics of the bypass system are reported in reference 7.

Three diffuser terminations were studied during this investigation and are shown schematically in figure 3. The inlet was terminated at the diffuser exit (1) by a long cold-flow pipe, with the internal flow choked at the exit plug located 92.9 inches (236 cm) from the compressor-face measuring station (station 2 in fig. 3); (2) by a choke plate positioned 4.5 inches (11.4 cm) downstream of the compressor-face measuring station; and (3) by a J85-GE-13 turbojet engine (the inlet guide vanes are 5.86 inches (14.9 cm) from the compressor-face measuring station). The total internal volume of the coldpipe

configuration was 15.1 cubic feet (4.3 $m^3$). Volume forward of the choke plate was 5.9 cubic feet (1.7 $m^3$). Details of the choke plate are shown in figure 4. Its total flow area of 84.5 square inches (545.0 $cm^2$) was sized to cause the inlet to operate at the peak recovery (or minimum stable) point with about 1.0 percent of the inlet capture mass-flow ratio controlled by the overboard bypass.

The J85-GE-13 turbojet engine had an eight-stage axial-flow compressor with a sea-level static average pressure ratio per stage of 1.275 for military power operation. This yields an overall pressure ratio of 7.0. The compressor was driven by a two-stage turbine. The compressor interstage bleed valves and the inlet guide vanes provided variable geometry for the compressor. Bleed was located in the stators of the third, fourth, and fifth compressor stages. Steady-state engine operation with this inlet is discussed in detail in reference 4. Transient inlet-engine interactions are reported in reference 3.

The inlet nacelle was mounted adjacent to the plate with a strut fairing between the nacelle and the plate as shown in figure 5. The strut fairing was a $12^o$ included angle wedge (fig. 5(b)) and was attached to the plate. Spacers were inserted between the strut fairing and plate to increase the cowl-lip-to-plate spacing from the minimum distance of 4 inches (10.2 cm) (shown in fig. 5) to a maximum of 7 inches (17.8 cm). The bottom of the strut fairing was machined to fit the inlet external cowl contour and was covered with a rubber pad to prevent damage to the nacelle during alinement of the independently mounted nacelle and plate. An overall view of the installation is shown in figure 6. The plate spanned the test section and had an overall length of 18 feet (5.49 m). The nacelle and plate were positioned for each strut fairing spacer height to place the external cowl against the rubber pad and keep the inlet at $0^o$ angle of attack relative to the plate. Vertical translation of the plate and the inlet nacelle was not possible. Therefore to vary the spacer height the plate and nacelle were rotated to negative angles of attack so as to raise the plate aft end and lower the inlet cowl lip. The resulting negative plate angles of attack (relative to the free stream) of $0.3^o$ to $1.2^o$ caused slight variations in local Mach number with spacer height.

It was desired to vary the wing-boundary-layer thickness over a range to 4 inches (10.2 cm). The boundary-layer thickness on the smooth plate was about 2.38 inches (6.0 cm) at the cowl-lip station. A thicker boundary layer was artifically generated with four rows of small cylinders mounted vertical to the plate near its leading edge to increase the momentum deficit adjacent to the plate surface. The thickness of the artificially generated boundary layer was about 3.8 inches (9.7 cm) at the cowl-lip station. The installed cylinders can be seen in figure 6. The 15-foot (4.6-m) length between the plate leading edge and the inlet cowl lip was required to allow this momentum loss to evolve into a fully developed turbulent boundary layer. Details of the boundary-layer growth and the cylinder design are discussed in reference 1.

A section of the plate leading edge with cylinders installed is shown photographically

in figure 7. The arrangement of the cylinders is shown in the lower half of figure 8. Each cylinder was 0.96 inch (2.42 cm) high and had a diameter of 0.125 inch 0.3175 cm). The design momentum deficit required four of these cylinders per lateral inch. The cylinders were therefore axially spaced 1 inch apart in four rows to prevent local airflow blockage problems. The upper half of figure 8 shows the plate leading edge without cylinders, which was used to generate the thinner natural boundary layer. The profile for both these boundary layers is shown in figure 9.

## Instrumentation

Steady-state and transient instrumentation at the compressor-face measuring station is shown in figure 10. The inlet total-pressure recovery was determined from the six area-weighted rakes. The compressor-face transient pressure probe was located $75^{\circ}$ clockwise from the duct top centerline. This probe and the transient throat pressure probe (indicated in fig. 1 and located $30^{\circ}$ clockwise from vertical) were constructed with subminiature strain-gage transducers. The infinite line technique was used to obtain good frequency response to 1000 hertz. Each transducer was flush mounted to the inside diameter of the probe 3 inches from the probe entrance. The probe line was continued 25 feet aft of the transducer location (as described in ref. 8) to produce a nearly nonresonant line. Probe response was down 3 decibels at 1000 hertz.

The steady-state engine compressor discharge pressure was measured by 16 total-pressure probes mounted in four rakes as shown in figure 11. Two probes for measuring transient pressures were mounted adjacent to the two steady-state rakes located $30^{\circ}$ clockwise and counterclockwise from the top centerline. These probes used piezoelectric transducers mounted 6 inches aft of the probe entrance, followed by 15 feet of constant-diameter line aft of the transducer to approximate the infinite line. Response was down 3 decibels at 500 hertz, but relatively flat from 500 to 1000 hertz.

Forty-four steady-state static-pressure taps were flush mounted on the plate used to generate the wing boundary layer. These taps were used to determine the extent of inlet-shock and wing-boundary-layer interaction and the resulting overpressures for inlet-started and inlet-unstarted conditions. Tap locations are shown in figure 12. Thirteen strain-gage transducers were flush mounted on the plate (fig. 12) to determine shock and boundary-layer interaction effects during inlet unstart transients. Schlieren photographs of inlet unstart transients were obtained with a high-speed motion-picture camera operating at about 3000 frames per second.

## Test Procedure

The steady-state effects of inlet-shock and wing-boundary-layer interaction were recorded during inlet operation with the long coldpipe and choked plug. Transient inlet-shock and boundary-layer interactions were alternately determined with the long coldpipe, the choke plate, and the engine terminating the diffuser. Most unstart transients were initiated from the peak recovery or minimum stable inlet operating points. The minimum stable points are shown on the inlet performance curve (fig. 2). Peak inlet conditions were obtained by controlling the choked plug or the engine to reduce the main-duct corrected weight flow to 32.2 pounds per second (14.6 kg/sec) with 1 percent of the capture mass-flow ratio passing through the overboard bypass. The choke plate was also sized to pass a corrected weight flow of 32.2 pounds per second. Unstart was then accomplished by closing the overboard bypass doors with a step equivalent to a 0.004 decrease in mass-flow ratio. At Mach 2.3, unstarts were also initiated with the inlet operating supercritically, by overcontracting the inlet throat. The inlet spike was manually controlled for these tests. The spike could not be retracted enough to cause unstart at higher Mach numbers due to a physical travel limitation.

Inlet unstarts were also obtained by stalling the engine compressor. The procedure used to obtain compressor stall was as follows: Starting at a compressor pressure ratio near the engine normal operating line, incremental reductions in exhaust nozzle area were made. These reductions rematched the compressor to the turbine at higher compressor pressure ratios. Engine speed was held constant throughout this procedure by manually adjusting the throttle. Nozzle area reductions were continued until stall occurred. In order to avoid overtemperaturing the turbine during this procedure, the first-stage turbine stator area was reduced by 14 percent. This forced the compressor to operate at a higher than normal pressure ratio for each turbine inlet temperature. The compressor interstage bleed valves (mechanically linked to the inlet guide vanes) are normally scheduled by the main fuel control as a function of corrected speed. For stall attempts, the bleed valves were manually set to the maximum allowable bleed closure for safe engine operation. This procedure was required to obtain assurance of engine stall at corrected speeds below 94 percent. Exhaust nozzle blockage plates were required to force compressor stalls at engine speeds below 90 percent.

# DISCUSSION OF RESULTS

## Effect of Propulsion System Parameters on Inlet Unstart Transients

The maximum extent of inlet-shock and wing-boundary-layer interaction (or the boundary-layer separation resulting from shock expulsion) obtained during unstart tran-

sients is presented in figures 13 and 14. These data were obtained with the cowl lip just above the edge of the wing boundary layer. Figure 13 shows the profile of the interaction on the wing and figure 14 shows the most forward extent as measured on the inlet centerline and plotted against Mach number. Data are presented for unstarts initiated from peak inlet operation for each of the three diffuser terminations. Unstarts caused by engine stall are also shown.

Unstarts resulting from engine stall resulted in shock and boundary-layer interactions 2.4 to 2.8 inlet diameters forward of the inlet cowl lip. These results were about double the interaction extent obtained with bypass unstarts from peak recovery conditions. Interactions from the bypass unstarts ranged from 1.0 to 1.75 diameters forward of the cowl lip, and varied with diffuser termination. Inlet unstarts with the engine operating, which always resulted in compressor stall, caused a transient boundary-layer separation about 1.5 inlet diameters forward of the cowl lip.

It was determined, by extrapolating the data of figure 13, that transients resulting from inlet unstarts with the engine would require nacelles to be placed about 3.5 cowl-lip diameters apart (center to center) for no mutual interference. If the unstart was caused by engine stall, over 4 diameters would be required.

The effect of volume on shock expulsion distance is evident in figure 14 for the unstarts initiated from peak recovery. The long coldpipe increased boundary-layer separation 0.2 to 0.6 diameter forward of the separation distances obtained by the choke plate. Unstarts using the choke plate, presenting a volume smaller than that of the inlet-engine system, were less extensive than those with the engine (fig. 14). Unstarts using the long coldpipe, with a volume larger than presented by the engine, were less extensive than engine results at the lower Mach numbers and greater at the higher Mach numbers. Although the magnitude of the two choked volumes bracketed that of the inlet engine system, the results were not entirely consistent. A contributing factor may have been the additional effect of the hammershock following compressor stall which was not reproduced with the choked volumes.

Additional information on the effect of volume, and on the effect of the hammershock from stall, were obtained from the high-speed Schlieren motion-picture film. Figure 15 presents the transient boundary-layer separation against time as obtained from the film. Selected frames are shown in figure 16. The transient distance plotted on figure 15 was obtained from enlarged photographic prints by fairing or extrapolating the shock from the wing-boundary-layer separation into the wing surface. Both figures present data for unstarts at Mach 2.5 with each of the three diffuser terminations. With the engine installed, unstarts were initiated prior to compressor stall. Data are also presented for an unstart with the engine at Mach 2.3. Except for the unstart with the choke plate installed, the data in figure 15 are plotted only to the point where the disturbance was most extensive.

The rate of shock propagation for each of the Mach 2.5 transients was nearly iden-

tical during the first 12 to 13 milliseconds. The boundary-layer separation reached a distance of 1.3 to 1.4 cowl-lip diameters forward of the cowl lip in about 13 milliseconds for each of the diffuser terminations, as shown in figure 15. Schlieren photographs of the shock progression from zero to 13 milliseconds are shown in figure 16(b) for one of the Mach 2.5 unstarts. Photographs of the other Mach 2.5 unstarts during this period are not shown as they were identical in appearance. Thus, the unstart transients were relatively unaffected by the diffuser termination during the initial transient period. In fact, with all the unstart transients obtained with the engine installed, evidence of stall (i.e., the hammershock) was not detected passing the inlet cowl lip until 12 to 13 milliseconds after the unstart was initiated. This same time delay of the hammershock occurred when the unstart was caused by compressor stall. Techniques to control the effects of engine stall for this size model must therefore be effective within a 13-millisecond time span.

Beyond 13 milliseconds, events were controlled by the diffuser termination as shown by the divergence of the three Mach 2.5 unstart curves in figure 15. The different shock patterns that appeared at the beginning of the divergence are illustrated at about 13.6 milliseconds in figures 16(a) to (c). The transient boundary-layer separation from unstart using the inlet choke plate configuration peaked at about 13 milliseconds and receded thereafter (fig. 15). The shock pattern just after the peak at 13.6 milliseconds, as well as the receded shock at 18.1 milliseconds, is shown for this configuration in figure 16(a). The transient separation from unstart using the inlet coldpipe configuration continued to move forward, as would be expected from the steeper cone shock at 13.6 milliseconds (fig. 16(b)) and peaked at 16.4 milliseconds (figs. 15 and and 16(b)). This larger transient appears to be due to the larger volume of the inlet-coldpipe combination.

When unstarts were made with the engine operating, the compressor stalled, as noted previously. The effect of the expelled hammershock following the stall was to overtake the existing unstarted shock structure at about 13.6 milliseconds and further expel the wing-boundary-layer separation (fig. 15). The hammershock formed into a normal shock at the cone tip at 13.6 milliseconds, and the peak of the boundary-layer separation at 18.0 milliseconds is shown in figure 16(c). Better photographic coverage of an emerging hammershock was obtained during the unstart at Mach 2.3 with the inlet operating supercritically. Figure 16(d) illustrates this case and shows the hammershock crossing the spike to form a normal shock at the spike tip less than 3 milliseconds after passing the cowl lip. Although the hammershock reached the spike tip at 14 to 15 milliseconds, the peak extent of the wing-boundary-layer separation did not occur until after the hammershock had receded; for example, at 18 and 21.3 milliseconds as shown in figures 16(c) and (d).

Unstarts were made from supercritical inlet operation at Mach 2.3 by overcontracting the throat. With all three diffuser terminations, the extent of boundary-layer sepa-

ration peaked about 0.5 cowl diameter forward of the cowl lip at about 6 milliseconds. This is shown in figure 15 for the supercritical unstart with the engine. With the choked volumes this peak was the maximum extent of the disturbance. However, with the engine installed, a second and much larger peak occurred at a later time (as a result of the hammershock) as shown in the figure. A summary of all the results obtained at Mach 2.3 is presented in figure 17. The maximum transient boundary-layer separation is presented for various initial inlet total-pressure recoveries. Data are shown for unstarts using the three diffuser terminations and unstarts resulting from engine stall. The maximum extent of separation with the choked volumes remained near 0.5 for all supercritical unstarts but was twice as great for unstarts near critical (above a recovery of 0.9). During the supercritical transients the magnitude of the transient appeared to be governed by the small volume forward of the choked inlet throat. Operation too near critical however caused the choke point to transfer aft and resulted in the larger transients associated with the greater volume of the diffuser or diffuser plus coldpipe.

When unstarts were initiated by, or resulted in, engine stall, the maximum extent of transient boundary-layer separation was governed not by internal volume but by the hammershock effects of compressor stall. Figure 17 again shows that the extent was greater with stall causing unstart than it is with unstart causing stall. It is apparent in the figure that the magnitude of the disturbance tended to increase with increases in engine speed. A much better correlating parameter, which reflects engine conditions by its relation to the compressor operating map, was found to be compressor mass-flow ratio. As shown in figure 18 the maximum extent of boundary-layer separation correlated well with compressor mass-flow ratio at the instant of stall. For unstart causing stall, the mass-flow ratio at stall was determined by correcting the steady-state ratio measured prior to the transient. The correction accounted for the compressor-face total-pressure-recovery loss during the unstart portion of the transient as recorded by the transient instrumentation.

According to references 9 and 10 the peak transient compressor-face overpressure recorded during an engine stall (regarded as a direct measure of the stall magnitude) correlated well with the compressor exit pressure. A similar correlation for the data of the present test is shown in figure 19. When unstart preceded stall, the compressor pressure ratio plotted in figure 19 was determined from time histories of the transient instrumentation. The correlation of figure 19 seems at odds with the intuitive idea that a compressor stall acts much like a valve suddenly moved toward closed. In this interpretation it would seem that the reaction to the stall (or the overpressure) would correlate with the amount of mass flow suddenly denied passage. The overpressure would then correlate with the mass flow at the compressor face at the time of stall. In this interpretation it is difficult to understand why the compressor exit pressure should be a correlating factor.

An examination of the flow equations will show the relation between compressor exit pressure and engine mass flow. The engine corrected weight flow can be expressed as follows:

$$W_{corr} = m_2 \frac{\sqrt{\frac{T_2}{T_{ref}}}}{\frac{P_2}{P_{ref}}} = \text{Constant} \tag{1}$$

or

$$W_{corr} = K_1 \frac{m_2}{P_2} \sqrt{T_2} \tag{2}$$

where $K_1$ is a constant. Now a simple assumption is required: that the stall line of the engine is a straight line through zero-zero on the compressor map. This is expressed as follows:

$$\frac{P_3}{P_2} = K_2 W_{corr} \tag{3}$$

This assumption is very nearly correct for the zero distortion stall line of the J85 engine (ref. 11). After substituting equation (2) into equation (3),

$$\frac{P_3}{P_2} = K_3 \frac{m_2}{P_2} \sqrt{T_2} \tag{4}$$

By rearranging equation (4):

$$m_2 = K_4 \frac{P_3}{\sqrt{T_2}} \tag{5}$$

Thus correlations with compressor exit pressure are linked through the engine stall line to correlations with engine mass flow. Therefore, it seems likely that without large temperature variations, data correlating well with mass flow would also correlate well with compressor exit pressure.

It was assumed that total temperature was constant during the unstarts. The plot of figure 20, from data of the present test, is therefore an expected result. The absolute overpressure at the compressor face correlated well with absolute compressor-face

mass flow. The maximum transient boundary-layer separation did not correlate as well with absolute mass flow as with mass-flow ratio (fig. 18).

Three of the transients obtained during testing were selected for detailed study: (1) an unstart at Mach 2.5 from peak inlet pressure recovery with the engine operating, (2) an unstart at Mach 2.5 caused by engine stall, and (3) an unstart at Mach 2.3 from supercritical inlet operation with the engine operating. Analyses of these transients relied on the transient pressure instrumentation located from the compressor exit to the inlet cowl lip and on the high-speed schlieren motion pictures. The transient pressures are presented in figure 21 as a function of time. Since the transient instrumentation was very limited, the compressor-face and compressor-exit transducer outputs were corrected prior to the transients to equal the averaged steady-state values. The start of the transient (or time zero) was selected as the beginning of compressor-face pressure change. Time zero on the schlieren photographs obtained during unstarts (fig. 16) was selected as the frame prior to any emerging shock.

Data for the Mach 2.5 unstart from peak recovery is presented in figure 21(a). Unstart began at time zero and was primarily signaled by the fall of the compressor-face pressure. The compressor-exit pressure also decreased but at a slower rate. Because of this slower response, the ratio of compressor-exit to compressor-face total pressure (the compressor pressure ratio) began to rise. The initially slow fall of the inlet throat pressure was probably due to transient local flow effects in the throat region. External flow spillage began at about 2 milliseconds into the transient as the expelled shock structure moved forward of the cowl (fig. 16(b)). At this time the wing pressure near the cowl lip increased as the shock passed its location. The unstart part of the transient was completed. Without a further disturbance the shock would proceed forward to a maximum point as previously shown (figs. 16(a) and (b)) and then recede. However, at 6.5 milliseconds the compressor pressure ratio exceeded the zero distortion compressor stall line. The ratio peaked at a value of 4.82 at 8 milliseconds and thereafter fell precipitously indicating compressor stall. The resulting hammershock caused only a very small pressure blip at the compressor face at 10 milliseconds. No evidence of the hammershock passage was recorded by the throat pressure or the wing pressure, but it nevertheless passed the cowl at about 13 milliseconds. Its existence as an almost normal shock near the inlet spike tip is shown by the photograph in figure 16(c) at 13.6 milliseconds. The maximum extent of wing-boundary-layer separation occurred at 18 milliseconds, as shown in figure 16(c). The shock from the separated inlet spike boundary layer reached its first minimum at about this same time. This event coincided with a sharp peak in the wing pressure and a sudden rise in the inlet throat pressure.

The internal pressures recorded for the unstart caused by an engine stall are presented in figure 21(b). The stall was first detected by the rapid hammershock pressure rise at the compressor face resulting in a rapid decrease in the compressor pressure ratio. Loss of compression was also indicated by the decrease in compressor-exit

pressure at about 2 milliseconds. The hammershock reached the throat at 6.5 milliseconds, producing a sudden increase in the throat pressure. A maximum overpressure, 1.28 times the external flow field total pressure, was recorded at the compressor face at 10 milliseconds. The double-peak compressor-face pressure signature shown in figure 21(b) was typical of stall produced by this engine. The 8-millisecond time span between the peaks resulted from a stall zone that progressed circumferentially around the compressor face as it enlarged. The speed of rotation was about one-half of the engine rotor speed. This rotating stall was also reported in reference 3. The expulsion of the hammershock from the inlet at 11 milliseconds was recorded by the fall of the throat and compressor-face pressures, and by the sudden rise of wing pressure near the cowl lip. Although high-speed schlieren photographs were not obtained during stalls the external shock travel was traced with the wing transient pressures. The peak of the wing-boundary-layer separation occurred at 17 to 18 milliseconds. The initial transient pulse ended at 31 milliseconds.

As previously noted, the hammershock caused by stall with the inlet started (fig. 21(b)) required 6.5 milliseconds to travel from the compressor face to the throat, whereas the hammershock caused by stall following unstart (fig. 21(a)) required less than 3 milliseconds to travel the same distance. The 3-millisecond time was inferred by the use of the high-speed schlieren photographs which placed the hammershock at the cowl lip at 13 milliseconds. This disparity in hammershock travel time may be a result of unsymmetrical effects caused by the rotating stall and the relative circumferential locations of the single-tube instrumentation probes. These effects may be severe in the case of the present inlet configuration because the subsonic portion of the diffuser is divided into three sections by struts which extend aft to the compressor face.

Another time anomaly appeared when the hammershock transient time from the throat to the cowl lip of 4 milliseconds (fig. 21(b)) was compared to the throat-to-lip transient time of about 2 milliseconds obtained for the unstart shock (fig. 21(a)). It would be expected that the same time span would occur for both transients. This disparity also may be due to unsymmetrical effects.

Figure 21(c) presents the last transient to be analyzed. Pressures are presented for an unstart at Mach 2.3 with the engine operating and the inlet at a supercritical point. The initial fall of the throat total pressure prior to time zero was due to local flow changes as the inlet spike was manually ramped to cause throat overcontraction. At time zero the inlet-throat, compressor-face, and compressor-exit pressures decreased as unstart occurred. The unstart shock was observed to pass the cowl lip at about 2 milliseconds and the compressor pressure ratio began to rise. Events to this point in time were similar to the Mach 2.5 unstart case of figure 21(a). A noticeable difference was the smaller decrease in inlet pressures, reflecting a much milder unstart. As was previously discussed, the flow was choked at the inlet throat during supercritical operation. The small volume forward of the choke point produced a small

transient with a peak at about 6 milliseconds (fig. 15). The expelled shock structure reached its first minimum position at about 8 milliseconds, as indicated by the rise in the throat pressure of figure 21(c) at about this time. The pressure rise was higher than expected and the value of the pressure peak cannot be explained on a steady-state basis. The compressor pressure ratio continued to rise, exceeding the zero distortion stall line value of 6.9 at 4.5 milliseconds, and peaked at a value of 8.05 at 6.5 milliseconds. Stall was indicated by the rapid fall of compressor pressure ratio, the decrease of compressor-exit pressure, and the hammershock-induced compressor-face overpressure of 1.07 at 9 milliseconds. The hammershock reached the inlet throat at 11 milliseconds as signaled by the rise in inlet throat pressure. Expulsion of the hammershock from the inlet at 13 milliseconds was indicated by the peak of the throat pressure and the rapid rise of the wing pressure near the cowl (see fig. 16(d) at 13.6 msec). The peak of the transient as measured by the maximum extent of wing-boundary-layer separation occurred at 21.3 milliseconds (fig. 16(d)). The peak in the near-cowl wing pressure and the sudden rise in inlet throat pressure at about 20 milliseconds coincided with the second minimum position of the shock from the separated inlet spike boundary layer.

## Effect of Airframe Installation on the Extent of Inlet-Shock and Boundary-Layer Interaction

The inlet-coldpipe combination was utilized to determine the effects of installation resulting from variations in boundary-layer thickness and wing-to-cowl-lip spacing. Three wing-to-cowl-lip spacings were investigated while using the thick boundary layer. The forward extent of shock and wing-boundary-layer interaction for these conditions is presented in figure 22 as a function of Mach number. Data are shown for the inlet started, the inlet unstarted but stable, and the unstart transients from peak recovery conditions. The unstarted inlet was not stable after the peak of the unstart transients. See figure 21 for example. Stable operation was achieved by reducing the inlet back pressure until the throat choked. Profiles of the interaction on the wing surface at Mach 2.5 are presented in figure 23 for the smallest and largest wing-to-cowl-lip spacings. As was expected, the extent of the inlet-shock and wing-boundary-layer interaction was reduced by increasing the wing-to-cowl-lip spacing. An increase in spacing from about 1.1 boundary-layer heights ($0.223\ h/D_c$) to 1.9 heights ($0.382\ h/D_c$) decreased the forward extent of the transient boundary-layer separation by as much as 0.4 cowl diameter, and reduced the extent of the interaction about 0.2 cowl diameter during stable inlet conditions (fig. 22). The lateral extent of interaction was also reduced about 0.2 diameter during unstarted stable inlet operation for the same increase

in wing-to-cowl-lip spacing (fig. 23). Extrapolation of the data of figure 23 indicates that the increase in wing-to-cowl-lip spacing reduced the lateral extent of the transient interaction such that an adjacent inlet could be placed about 0.5 cowl diameter closer without being affected by the unstart.

Profiles of the shock and boundary-layer interactions obtained for stable and transient conditions with the cowl lip near the edge of the boundary layer are presented in figure 24 for Mach numbers 2.3 to 2.6. The centerline extent of these profiles reflect the Mach number trends of figure 22. The indicated increase in transient magnitude with increasing Mach number resulted from the increase in unstart severity with larger amounts of internal contraction. The extent of shock and boundary-layer interaction during inlet-started conditions receded as Mach number was increased since the spike position was retracted and the Mach angle was reduced. Placement of side-by-side inlet nacelles for no mutual interference during unstarts with the long coldpipe would require center-to-center spacings of 3 to 4 cowl diameters over the Mach number range of figure 24. With the engine operating, unstarts prior to stall required about the same spacing for no interference (about 3.5 diameters, as was shown in fig. 13), whereas unstarts caused by stall would require a larger spacing of over 4 diameters (fig. 13). Elimination of the large transient effects could reduce nacelle placement for no interference to the unstarted stable value of about 2 center-to-center diameters. If unstarts could be prevented, figure 24 shows that interference from the inlet-shock structure need not be considered in nacelle placement.

The effects of variations in boundary-layer thickness were determined by testing with the artificially thickened boundary layer and the thinner natural boundary layer generated by the flat plate. The extent of shock and boundary-layer interaction produced by these two boundary layers was obtained with the long coldpipe diffuser termination during transient and steady-state inlet operation. The forward extent of the interactions is plotted in figure 25 as a function of Mach number, and the wing interaction profiles at Mach 2.5 are shown in figure 26. The cowl lip was placed at a fixed spacing ratio of $0.223\ h/D_c$ for these comparisons. As expected, the maximum forward extent of boundary-layer separation resulting from coldpipe unstarts was less with the thin boundary layer by 0.2 to 0.5 cowl diameter over the Mach number range. The forward extent of the interaction during steady-state or stable inlet operation was also reduced about 0.2 diameter with the thinner boundary layer. The relatively large effect of boundary layer on the interaction location from the conical shock of the started inlet was initially unexpected since the shock strength was insufficient to separate the wing-flow-field boundary layer. However, the location of the interaction was aft of the cowl, where the combined effects of the external cowl, the strut fairing, and the centerbody shock waves were sufficient to cause separation. The separation was observed on a single schlieren photograph where the cone shock just entered the strut fairing region. With the thinner boundary layer, the lateral extent of the interaction was also less than that with the thick

boundary layer. Extrapolation of the unstart transient curves of figure 26 indicate that the nacelle spacing for no mutual interference could be decreased by about 0.75 cowl diameter with the thin boundary layer.

The extent of the inlet-shock and boundary-layer interaction resulting from the two boundary layers was also compared for a wing-to-cowl-lip spacing fixed at about 1.8 times the boundary-layer height. As shown in figure 27, the forward extent of the interactions obtained with the thinner boundary layer was only slightly less than that obtained with the thick boundary layer when compared in this manner.

Reference 1 has reported on the separation characteristics of the thickened boundary layer used in this study. The characteristics were determined using a forward-facing step and were compared with other available data on natural boundary layers. The results indicated that the thickened boundary layer tended to separate about one boundary-layer height too far forward at the higher Mach numbers used in this test (i.e., 2.5 and 2.6). However, figure 27 shows that the forward extent of separation obtained with the thickened boundary layer had the same Mach number trend as the thinner natural boundary layer.

Figure 28 presents typical shock and boundary-layer interaction profiles obtained for the wing-to-cowl-lip spacing fixed at 1.8 times the boundary-layer height. The lateral extent of the disturbance was less with the thinner boundary layer. Therefore, nacelle placement for no mutual interference during transients could be decreased by about 0.5 cowl diameter.

## Steady-State Performance

Figure 29 presents the critical inlet performance as a function of wing-flow-field Mach number. Data are shown for the inlet cowl lip at various spacings to the wing and for the two wing boundary-layer heights. Fairings connect the data obtained with each boundary-layer thickness at each nominal Mach number. The data trend with Mach number within each grouping was attributed to Mach number effects at a constant spike setting. Over the Mach number range tested there did not appear to be any performance degradation resulting from moving the inlet lip in to about one boundary-layer height from the wing. Lower inlet total pressure and higher distortion were recorded when the inlet was tested with the thicker, rather than the natural, boundary layer. This resulted from an inviscid loss of total pressure in the wing flow field created by the shock from boundary-layer generators at the plate leading edge. The internal area ratio at which the inlet could be restarted was also unaffected by moving the cowl lip in to about one boundary-layer height from the wing. This is shown in figure 30, where the restart area ratios obtained for all test conditions are plotted and compared to the measured restart area ratios obtained without an adjacent wing in reference 6.

## Transient and Steady-State Wing Pressures

Maximum wing pressures recorded during unstart transients with the cowl lip near the edge of the scaled boundary layer are presented in figures 31 and 32. Figure 31 shows the pressures recorded by the centerline and off-centerline pressure probes at Mach 2.5, and figure 32 presents the pressure just forward of the cowl lip as a function of Mach number. Data are shown for engine stalls and for unstarts from peak recovery conditions with the three diffuser terminations. The profiles revealed that the peak transient wing pressures occurred at the inlet cowl-lip location and were very much higher than the maximum pressures in other areas of the separated region. At Mach 2.5 (fig. 31) the near-cowl-lip pressures were about 6 to 10 times the wing-flow-field static pressure. In other areas of the separation field, the maximum pressure recorded for any of the transients was about 2.5 times the static pressure. Although considerable scatter occurred in the peak pressures (fig. 32), the pressure trends with Mach number and with configuration were generally similar to the trends exhibited by the maximum transient boundary-layer separations obtained with the unstart-from-peak configurations (fig. 14). The peak pressures recorded following unstart from engine stall did not continue the similarity. Whereas the transient boundary-layer separations from stall were about twice as extensive as those from unstarts (fig. 14), the peak pressures from stalls were only slightly higher than those from unstarts. Peak transient pressures were limited to about 7 to 10 times the wing static pressure over the Mach number range.

The amount of transient wing pressure instrumentation was insufficient to determine detailed wing-static-pressure distributions during the peak of transients. Pressure contours were determined from steady-state instrumentation for stable conditions with the inlet unstarted. These are presented in figure 33 for the thick and the thin boundary layers with the wing-to-cowl-lip spacing ratio fixed at the minimum distance tested of 0.223 cowl diameter. A projection from these plots suggest that the maximum wing pressures were located adjacent to the strut fairing about 0.3 diameter aft of the cowl lip. At each Mach number the thickened boundary layer produced maximum pressures in the separated region that were about $0.2\ p_w$ lower than the pressures produced by the natural boundary layer. These results are in agreement with those of reference 1, which reported pressure in the separation region of this thickened boundary layer to be $0.15$ to $0.3\ p_w$ lower than the pressure obtained with natural boundary layers.

## SUMMARY OF RESULTS

A Mach 2.5 nacelle-mounted inlet was placed adjacent to a simulated wing boundary layer. The extent of interaction between the inlet shock and wing boundary layer was

determined for normal inlet operation, unstarted inlet operation, and unstart transients. Unstart transients were initiated with bypass closure, throat overcontraction, or stall of the J85-GE-13 turbojet engine. Unstarts were also obtained for an inlet and coldpipe combination, and for an inlet with a choke point at the compressor face, as well as for the inlet-engine combination. The effects of boundary-layer height and wing-to-cowl-lip spacing were determined. The test was conducted in the Lewis 10- by 10-Foot Supersonic Wind Tunnel over a Mach number range of 2.3 to 2.7 with the following results:

1. Inlet unstarts following engine stall resulted in transient-shock and wing-boundary-layer interactions 2.4 to 2.8 cowl-lip diameters forward of the cowl lip. Unstarts resulting from bypass closure caused engine stall but produced smaller separation distances of about 1.5 diameter forward of the cowl lip.

2. The lateral extent of transient separation caused by engine stall would require adjacent nacelles to be separated by over 4 cowl-lip diameters for no mutual interference.

3. With an engine installed, the magnitude of the transient separation was controlled by the compressor stall hammershock and correlated with the engine-face mass-flow ratio at the instant of stall, whether stall caused unstart or stall followed unstart.

4. The transient magnitude as measured by the hammershock overpressure at the compressor face correlated with the absolute engine-face mass flow at stall. Overpressure also correlated with the compressor-exit pressure through its relation to mass flow described by the engine stall line.

5. The hammershock following engine stall was observed emerging from the inlet 12 to 13 milliseconds after the start of either a stall or an unstart.

6. When unstarts were initiated without an engine installed, the magnitude of the transient boundary-layer separation was found to vary with the internal volume forward of the choke point.

7. The maximum wing overpressure recorded during transients occurred locally near the cowl lip and was about 10 times the wing-flow-field static pressure.

8. As expected, the extent of the inlet shock and wing-boundary-layer interaction was reduced by increasing the wing-to-inlet distance or by reducing the boundary-layer thickness.

9. Started-inlet performance and the inlet restart cycle were unaffected by moving the cowl lip in to the edge of the wing boundary layer.

Lewis Research Center,
National Aeronautics and Space Administration,
Cleveland, Ohio, November 12, 1970,
720-03.

## REFERENCES


1. Johnson, David F.; and Mitchell, Glenn A.: Experimental Investigation of Two Methods for Generating an Artificially Thickened Boundary Layer. NASA TM X-2238, 1970.

2. Cubbison, Robert W.; Meleason, Edward T.; and Johnson, David F.: Effect of Porous Bleed in a High-Performance Axisymmetric, Mixed-Compression Inlet at Mach 2.50. NASA TM X-1692, 1968.

3. Choby, David A.; Burstadt, Paul L.; and Calogeras, James E.: Large-Scale Transient Interactions Between a Turbojet Engine and an Axisymmetric Inlet with 60-Percent Internal Area Contraction. NASA TM X-2192, 1970.

4. Coltrin, Robert E.; and Choby, David A.: Steady-State Interactions from Mach 1.98 to 2.58 Between a Turbojet Engine and an Axisymmetric Inlet with 60-Percent Internal Area Contraction. NASA TM X-1780, 1969.

5. Wasserbauer, Joseph F.: Dynamic Response of a Mach 2.5 Axisymmetric Inlet with Engine or Coldpipe and Utilizing 60-Percent Supersonic Internal Area Contraction. NASA TN D-5338, 1969.

6. Cubbison, Robert W.; Meleason, Edward T.; and Johnson, David F.: Performance Characteristics from Mach 2.58 to 1.98 of an Axisymmetric Mixed-Compression Inlet System with 60-Percent Internal Contraction. NASA TM X-1739, 1969.

7. Neiner, George H.: Servo System Design of a High Response Slotted Plate Overboard Bypass Valve for a Supersonic Inlet. NASA TN D-6081, 1970.

8. Wilhelm, Walter E.: Investigation of Tubing Effects on Amplitude Frequency Response of Pressure Sensing Systems Using Nonresonant Terminations. NASA TM X-1988, 1970.

9. Bellman, Donald R.; and Hughes, Donald L.: The Flight Investigation of Pressure Phenomena in the Air Intake of an F-111A Airplane. Presented at the AIAA 5th Propulsion Joint Specialist Conference, U.S. Air Force Academy, Colorado, June 9-13, 1969.

10. Morriss, D. P.; and Williams, D. D.: Free-Jet Testing of a Supersonic Engine/Intake Combination. Aeronautical J., vol. 74, no. 711, Mar. 1970, pp. 212-218.

11. Calogeras, James E.: Experimental Investigation of Dynamic Distortion in a Mach 2.50 Inlet with 60-Percent Internal Contraction and Its Effect on Turbojet Stall Margin. NASA TM X-1842, 1969.

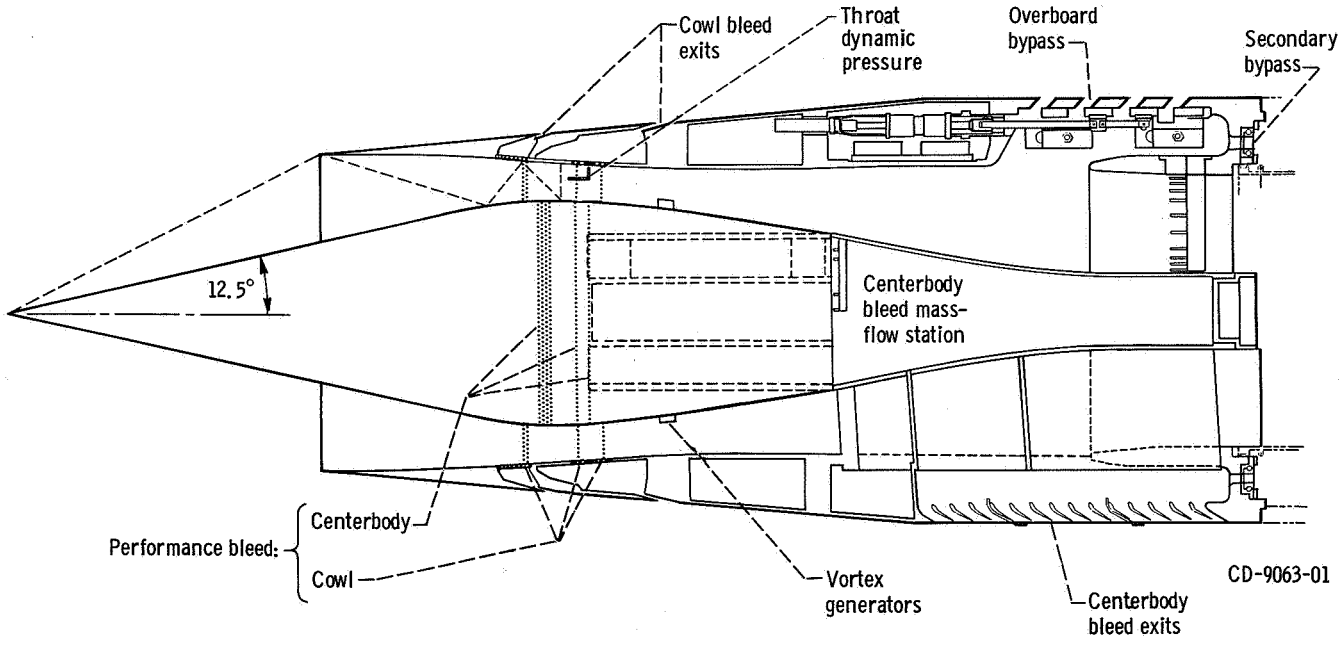


Figure 1. - Cross section of axisymmetric Mach 2.5 mixed-compression inlet.

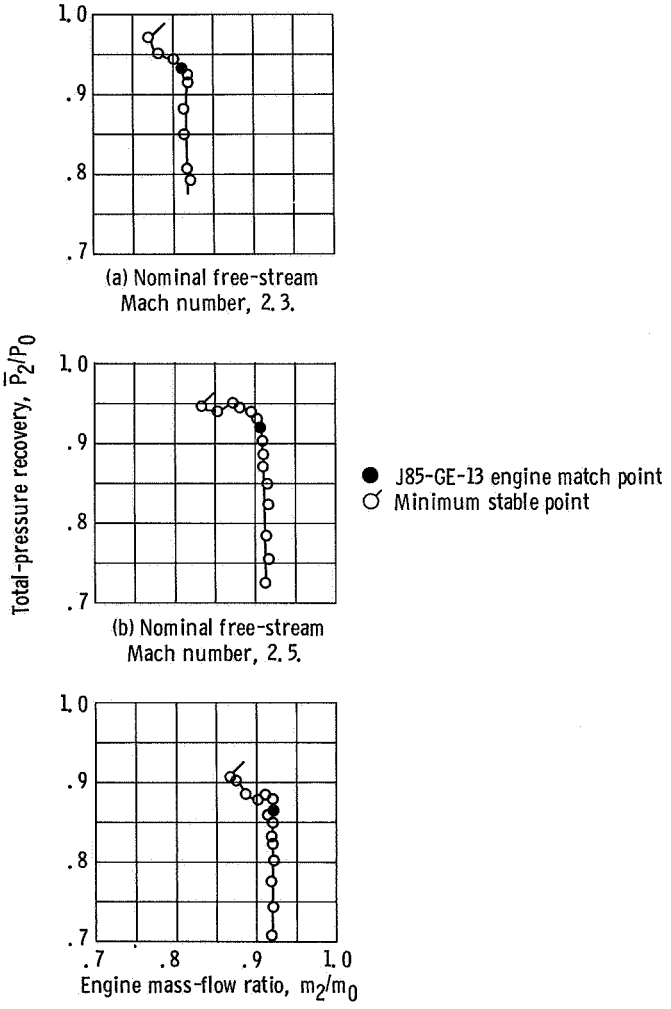


Figure 2. - Performance of the Mach 2.5 mixed-compression inlet (ref. 6).

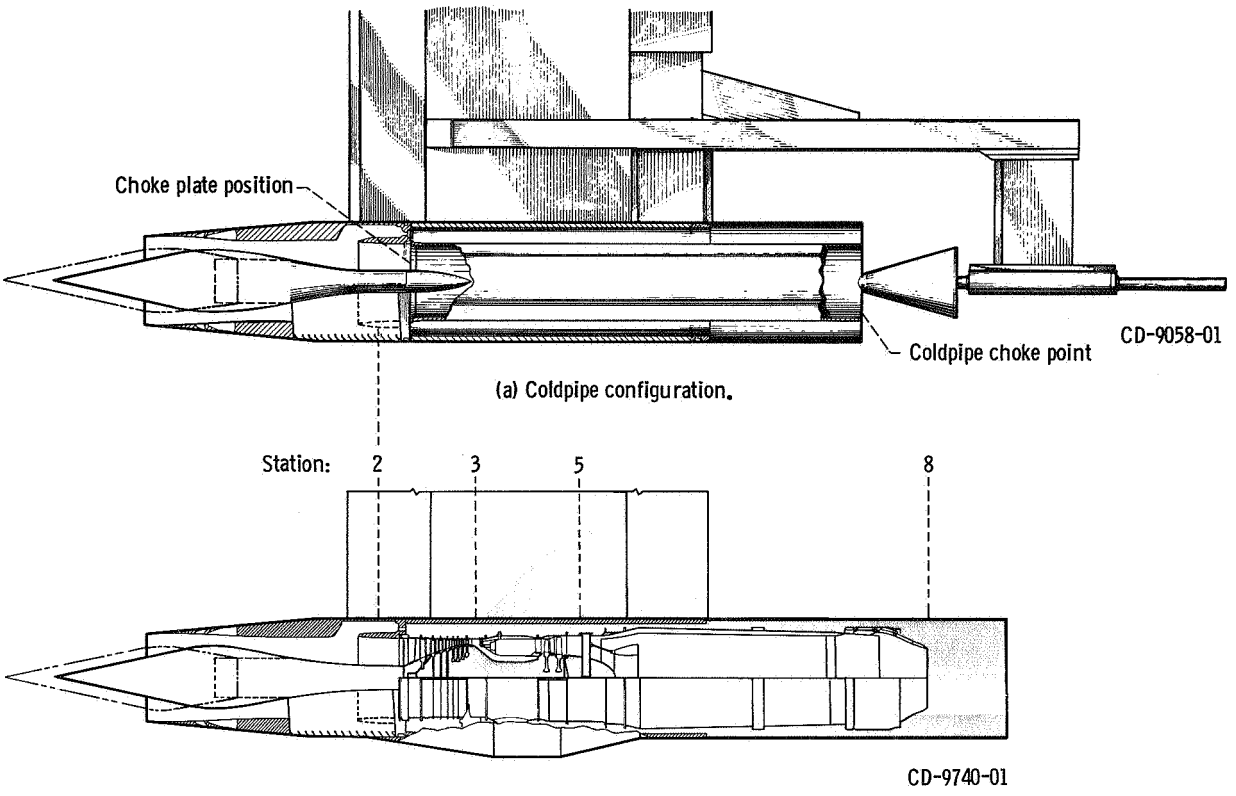


(a) Coldpipe configuration.

(b) Engine configuration.

Figure 3. - Cutaway of nacelle showing installation of coldpipe and J85-GE-13 turbojet engine.

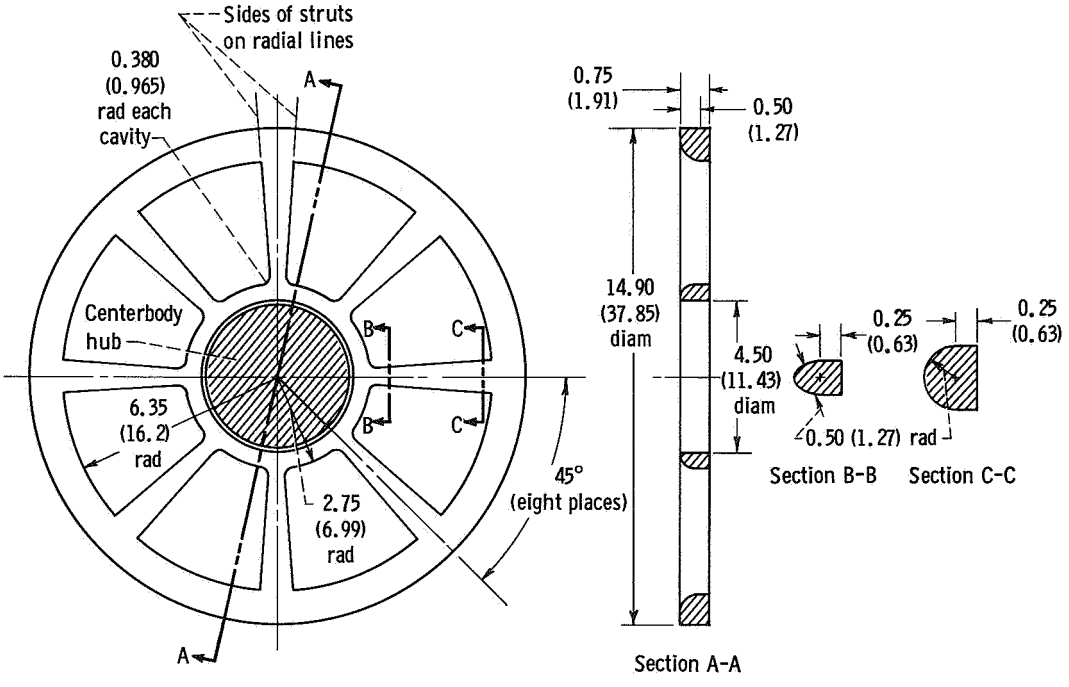


Figure 4. - Details of choke plate. Total area, 84.5 square inches (545.0 $cm^2$). (All dimensions are in inches (cm).)

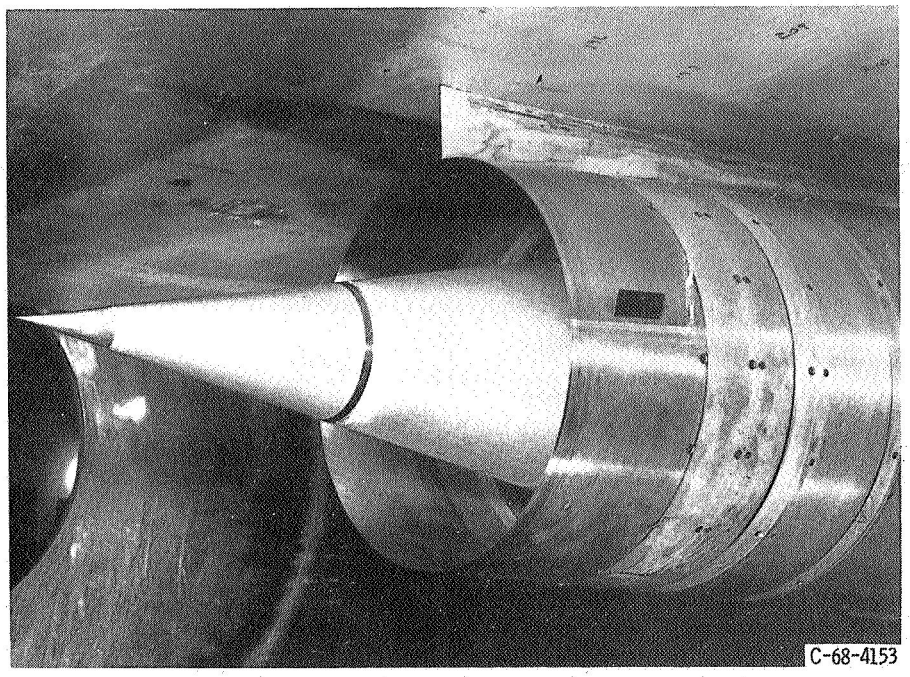


(a) Installed in wind tunnel.

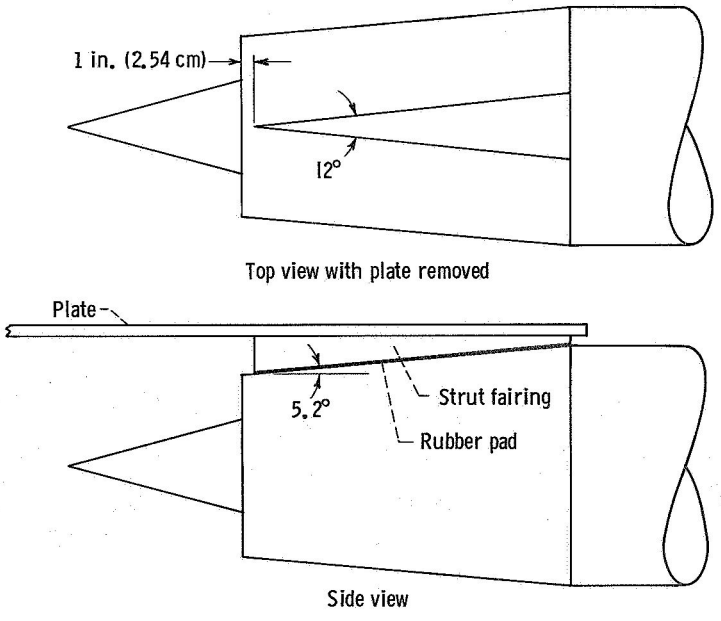


(b) Details.

Figure 5. - Inlet, strut fairing, and wing arrangement.

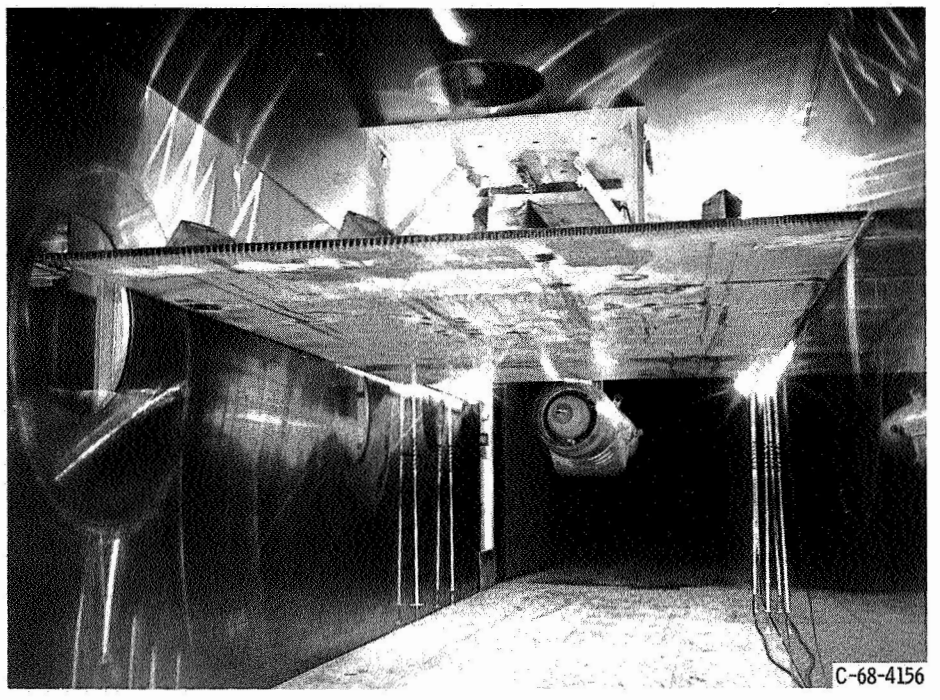


Figure 6. - Inlet-engine configuration and wing-boundary-layer simulation plate installed in 10-by 10-Foot Supersonic Wind Tunnel.

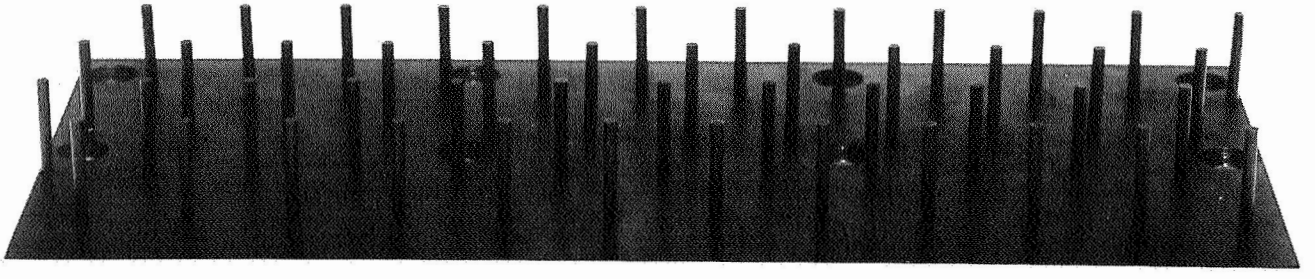

C-70-2187

Figure 7. - Cylinders used to thicken plate boundary layer.

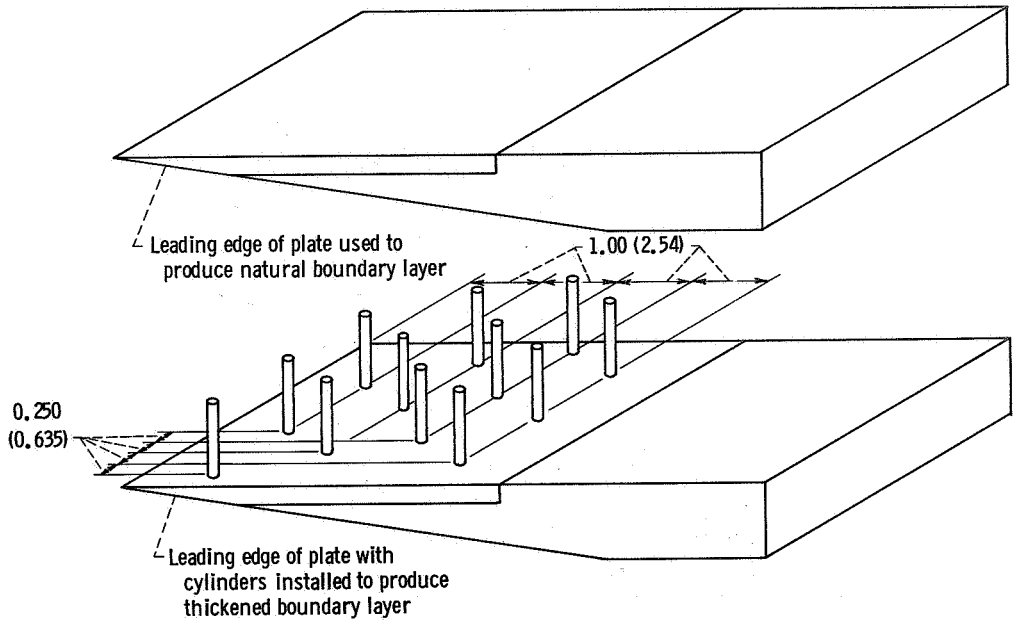


Figure 8. - Details of plate leading-edge configurations. Dimensions of all cylinders: diameter, 0.1250 inch (0.3175 cm); height, 0.96 inch (2.44 cm). (All dimensions are in inches (cm).)

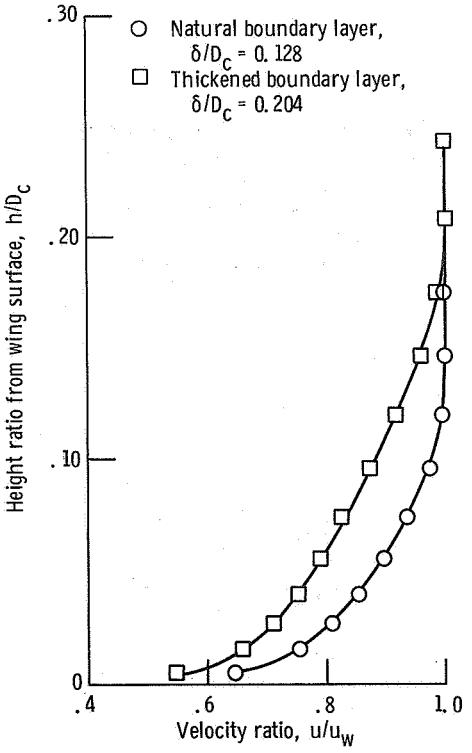


Figure 9. - Wing-boundary-layer profiles at inlet cowl-lip station. Mach number, 2.5.

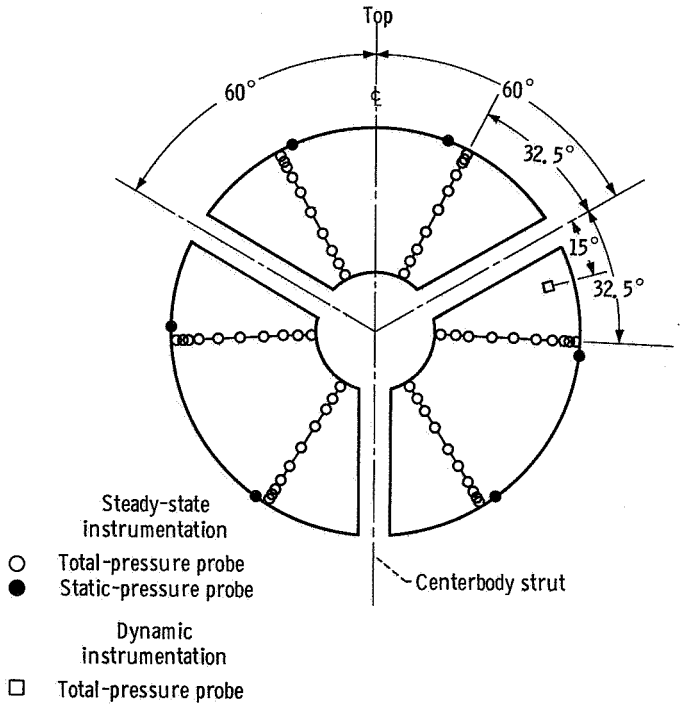


Figure 10. - Compressor-face (station 2) instrumentation, looking downstream.

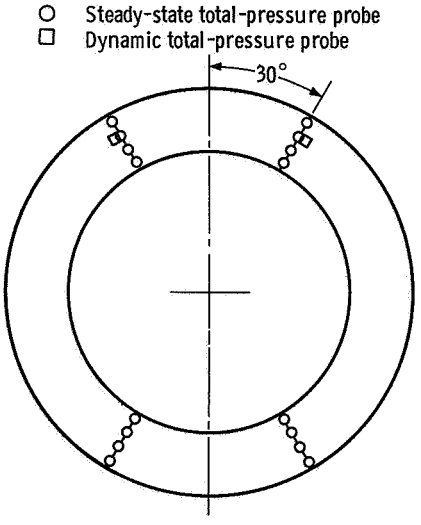


Figure 11. - J85-GE-13 engine compressor-exit (station 3) instrumentation, looking downstream.

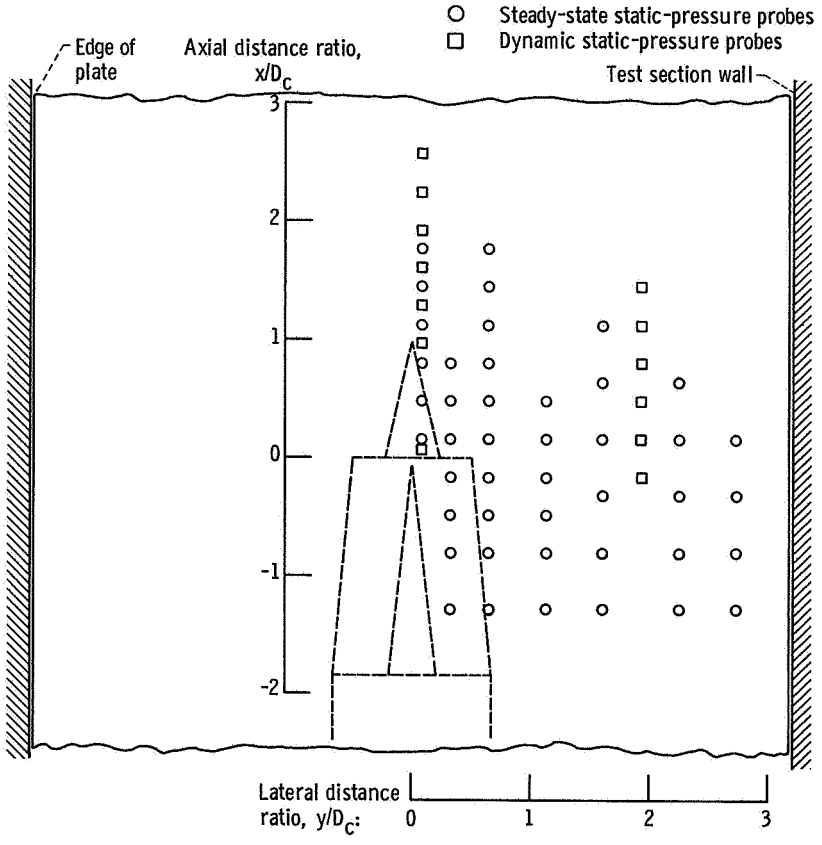


Figure 12. - Plate static-pressure instrumentation.

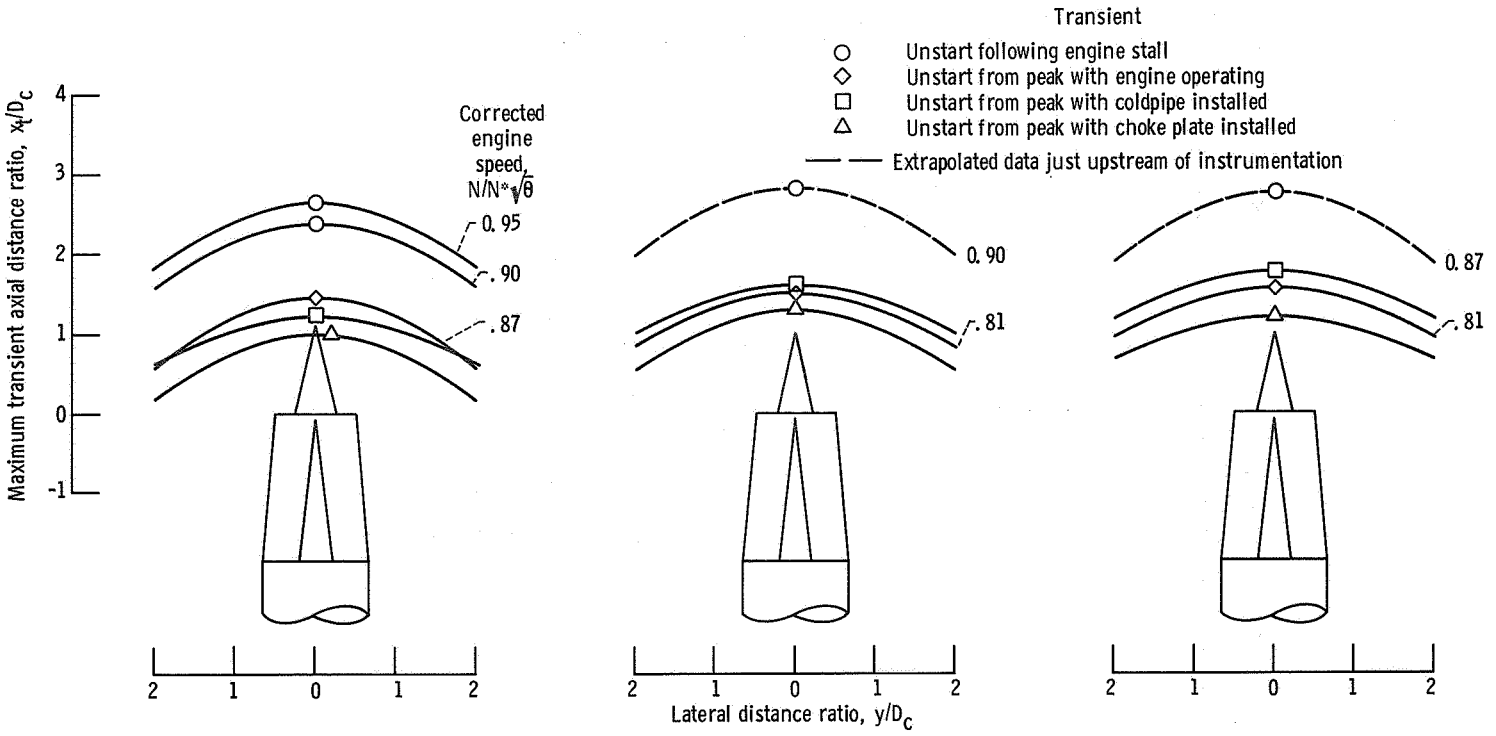


(a) Nominal Mach number, 2.3. (b) Nominal Mach number, 2.5. (c) Nominal Mach number, 2.6.

Figure 13. - Maximum extent of inlet-shock and wing-boundary-layer interaction during various unstart transients. Boundary-layer thickness parameter, $\delta/D_c = 0.204$; wing-to-cowl-lip spacing ratio, $h/D_c = 0.223$.

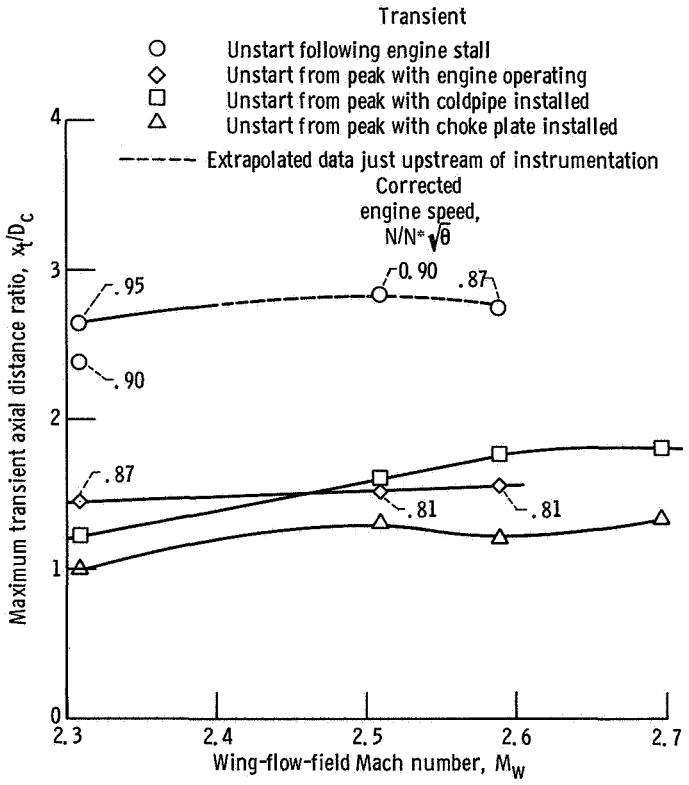


Figure 14. - Maximum forward propagation of inlet-shock and wing-boundary-layer interaction resulting from various unstart transients. Boundary-layer thickness parameter, $\delta/D_c = 0.204$; wing-to-cowl-lip spacing ratio, $h/D_c = 0.223$.

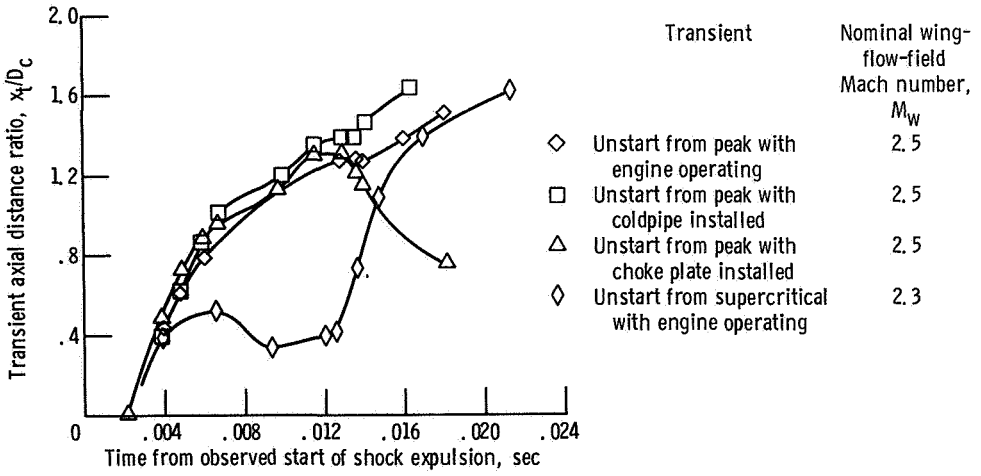


Figure 15. - Time history of forward propagation of transient inlet-shock and wing-boundary-layer interaction. Boundary-layer thickness parameter, $\delta/D_c = 0.204$; wing-to-cowl-lip spacing ratio, $h/D_c = 0.223$.

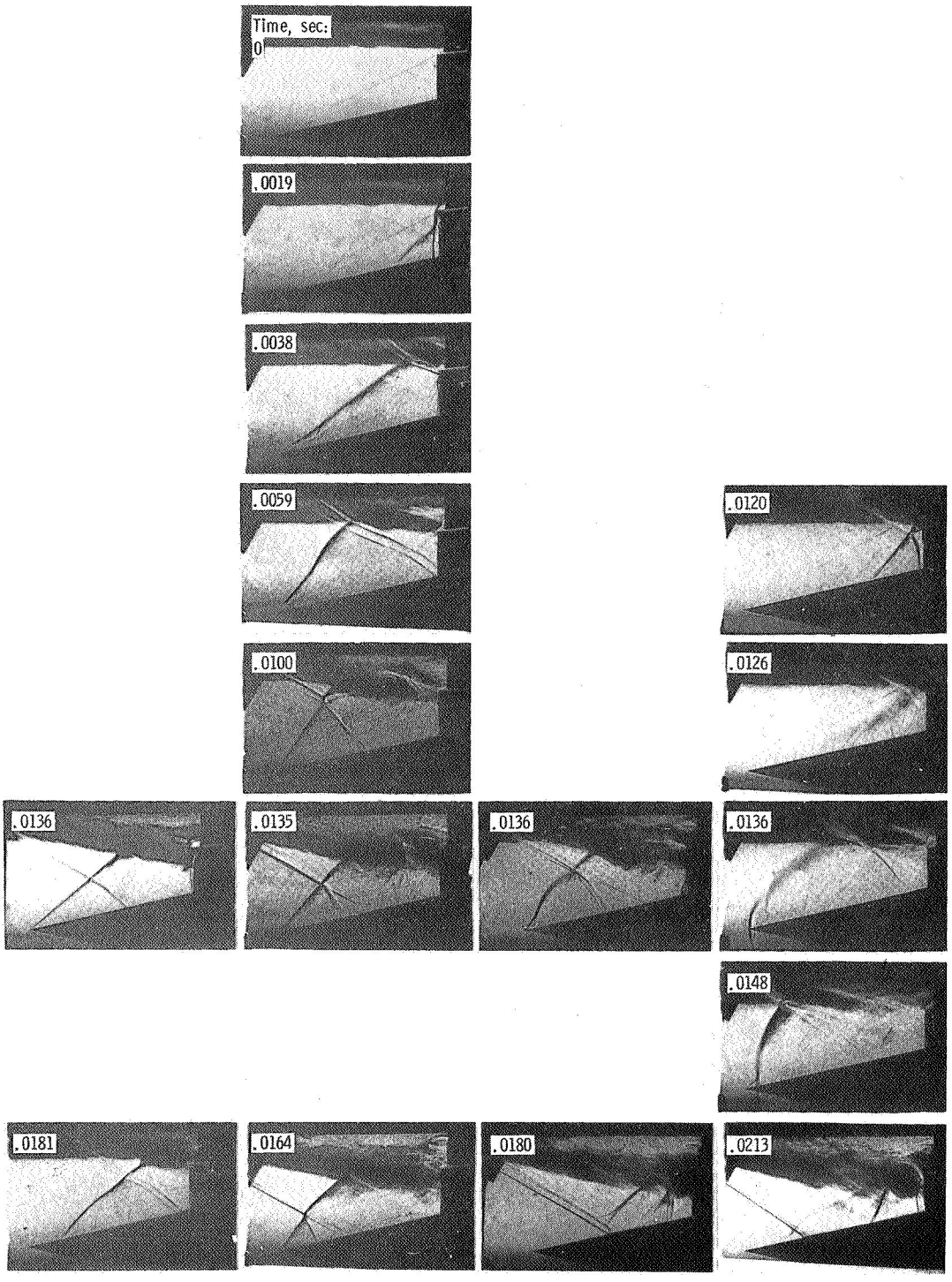


(a) Unstart from peak with choke plate installed. Nominal Mach number, $M_w = 2.5$.

(b) Unstart from peak with coldpipe installed. Nominal Mach number, $M_w = 2.5$.

(c) Unstart from peak with engine operating. Nominal Mach number, $M_w = 2.5$.

(d) Unstart from supercritical with engine operating. Nominal Mach number, $M_w = 2.3$.

Figure 16. - Selected schlieren photographs obtained during unstart transient. Boundary-layer thickness parameter, $\delta/D_c = 0.204$; wing-to-cowl-lip spacing ratio, $h/D_c = 0.223$.

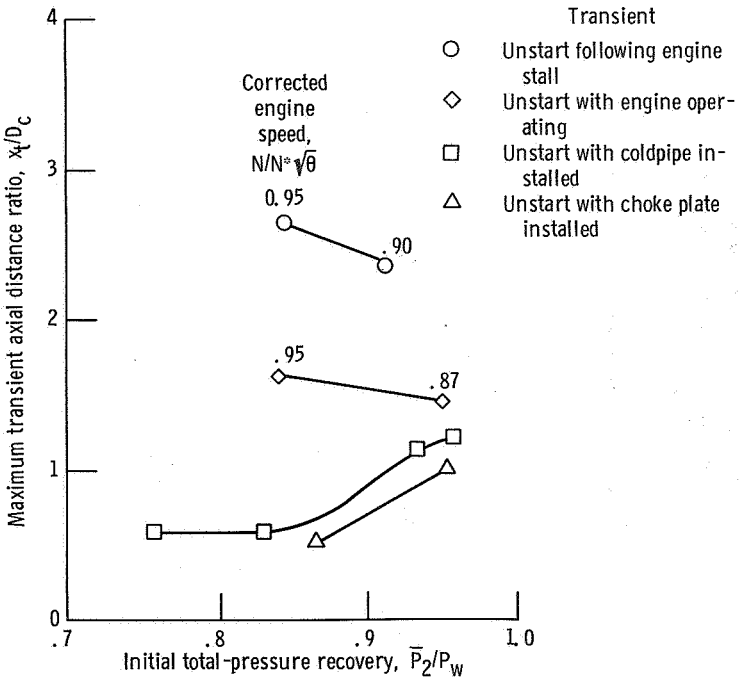


Figure 17. - Effect of initial inlet operating condition on maximum forward extent of inlet-shock and wing-boundary-layer interaction resulting from unstart transients. Nominal Mach number, $M_w = 2.3$; wing-boundary-layer thickness parameter, $\delta/D_c = 0.204$; wing-to-cowl-lip spacing ratio, $h/D_c = 0.223$.

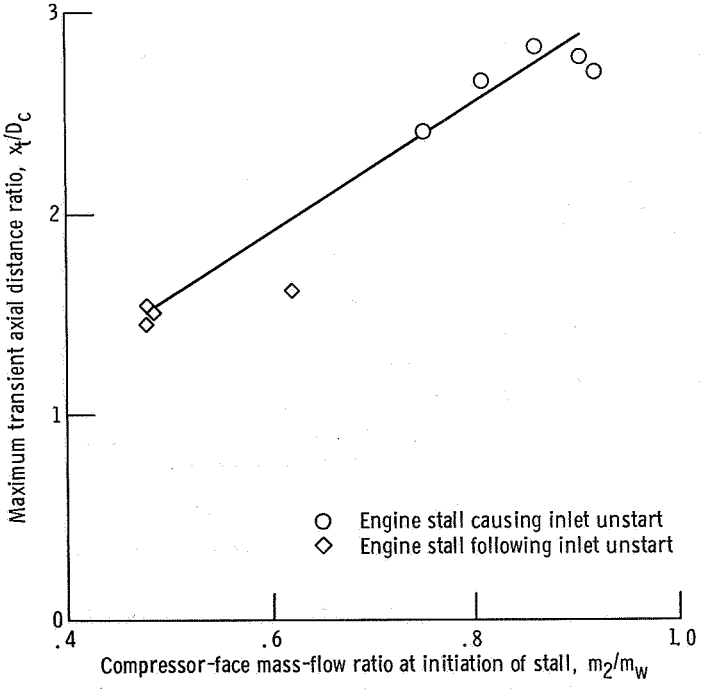


Figure 18. - Correlation of compressor-face mass-flow ratio at initiation of stall with maximum forward extent of transient-inlet-shock and wing-boundary-layer interaction. Wing-boundary-layer thickness parameter, $\delta/D_c = 0.204$; wing-to-cowl-lip spacing ratio, $h/D_c = 0.223$.

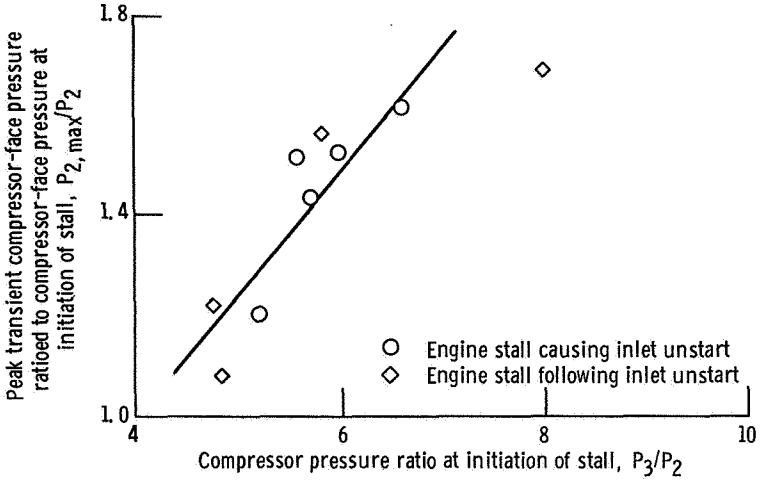


Figure 19. - Correlation of peak hammershock pressures with compressor-exit pressure.

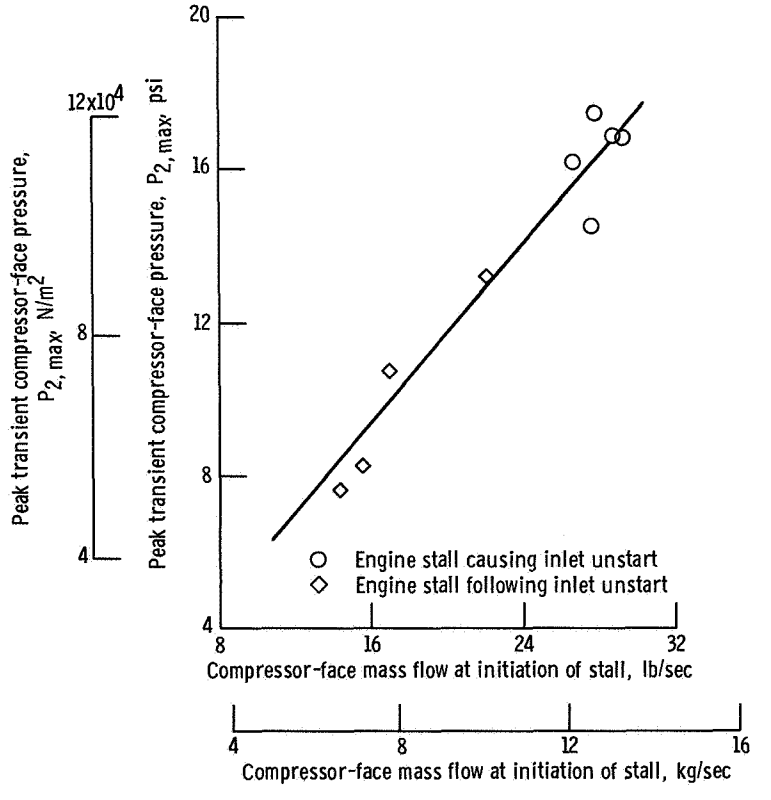


Figure 20. - Correlation of peak hammershock pressures with engine mass flow at initiation of stall.

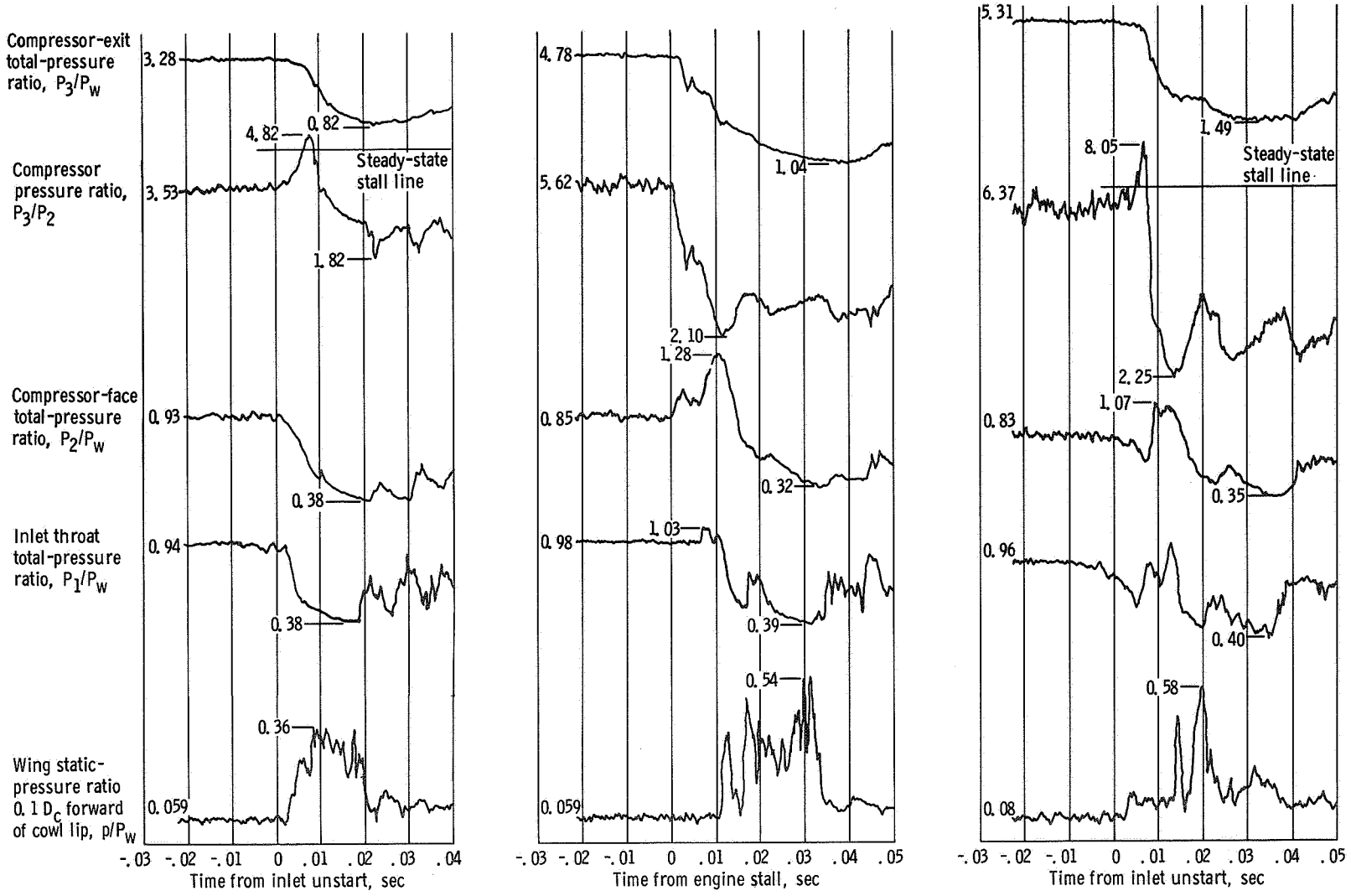


(a) Unstart from peak recovery with engine operating. Nominal Mach number, $M_w = 2.5$; corrected engine speed, $N/N^*\sqrt{\theta} = 0.81$; total-pressure recovery, $\bar{P}_2/P_w = 0.929$.

(b) Unstart following engine stall. Nominal Mach number, $M_w = 2.5$; corrected engine speed, $N/N^*\sqrt{\theta} = 0.90$; total-pressure recovery, $\bar{P}_2/P_w = 0.851$.

(c) Unstart from supercritical condition with engine operating. Nominal Mach number, $M_w = 2.3$; corrected engine speed, $N/N^*\sqrt{\theta} = 0.95$; total-pressure recovery, $\bar{P}_2/P_w = 0.834$.

Figure 21. - Pressure-time history during inlet unstart transient. Wing-boundary-layer thickness parameter, $\delta/D_c = 0.204$; wing-to-cowl-lip spacing ratio, $h/D_c = 0.223$.

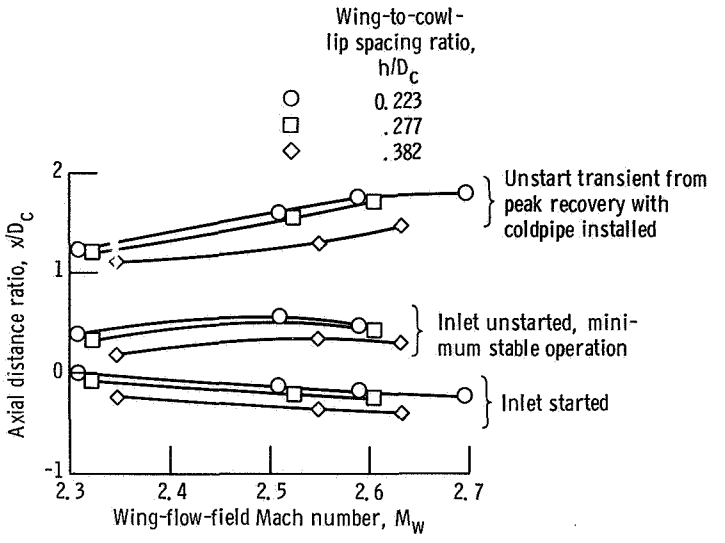


Figure 22. - Effect of wing-to-cowl-lip spacing on forward extent of inlet-shock and wing-boundary-layer interaction for a wing-boundary-layer thickness parameter, $\delta/D_c = 0.204$.

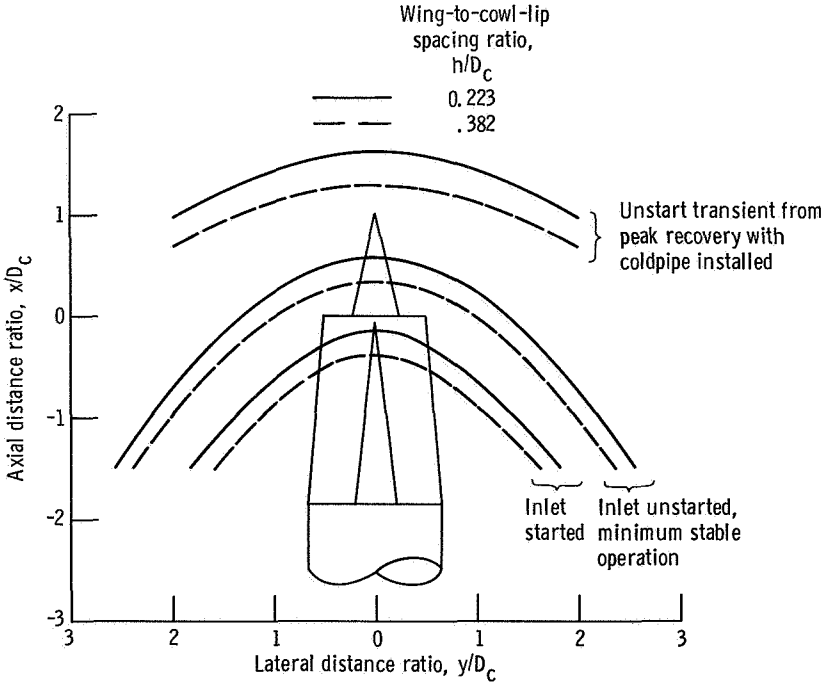


Figure 23. - Effect of wing-to-cowl-lip spacing on extent of inlet-shock and wing-boundary-layer interaction. Nominal wing-flow-field Mach number, $M_w = 2.5$; wing-boundary-layer thickness parameter, $\delta/D_c = 0.204$.

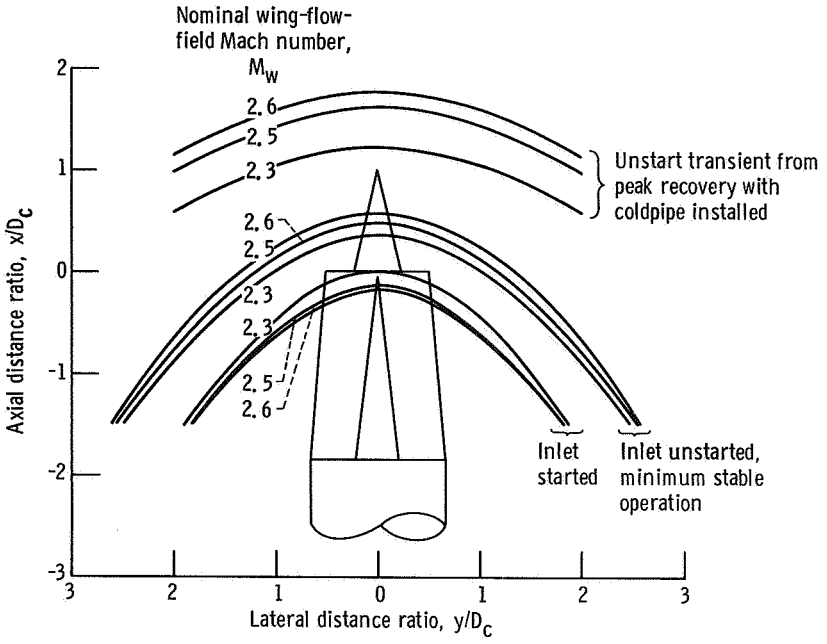


Figure 24. - Extent of inlet-shock and wing-boundary-layer interaction. Wing-boundary-layer thickness parameter, $\delta/D_c = 0.204$; wing-to-cowl-lip spacing ratio, $h/D_c = 0.223$.

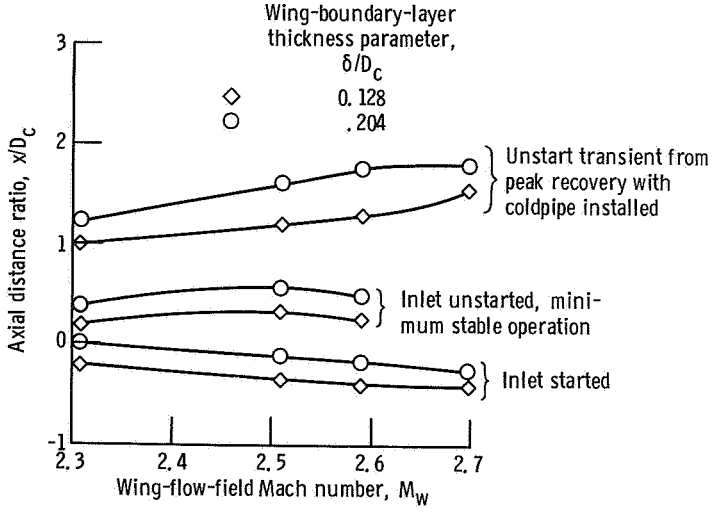


Figure 25. - Forward extent of inlet-shock and wing-boundary-layer interaction for two boundary-layer thicknesses. Wing-to-cowl-lip spacing ratio, $h/D_c = 0.223$.

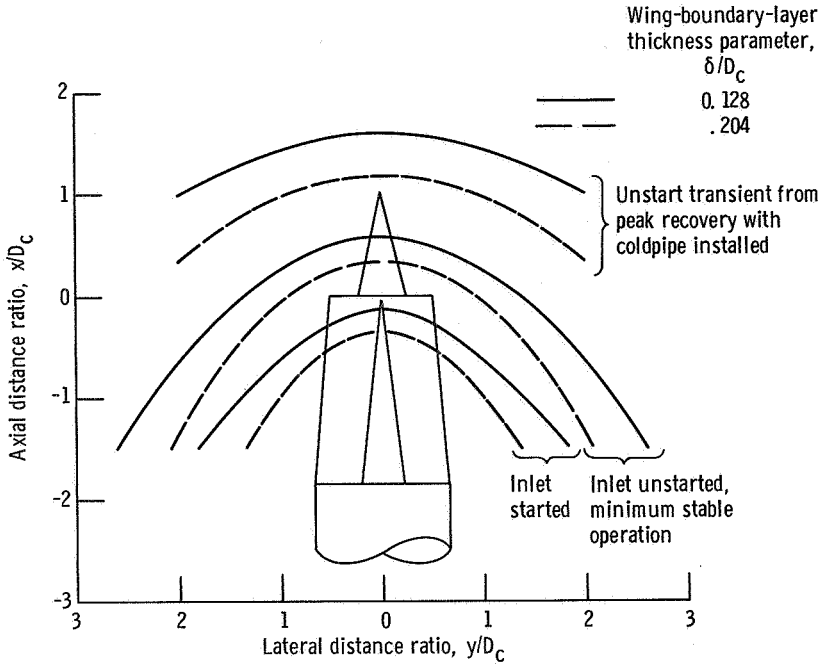


Figure 26. - Effect of boundary-layer thickness on extent of inlet-shock and wing-boundary-layer interaction. Nominal wing-flow-field Mach number, $M_w = 2.5$; wing-to-cowl-lip spacing ratio, $h/D_c = 0.223$.

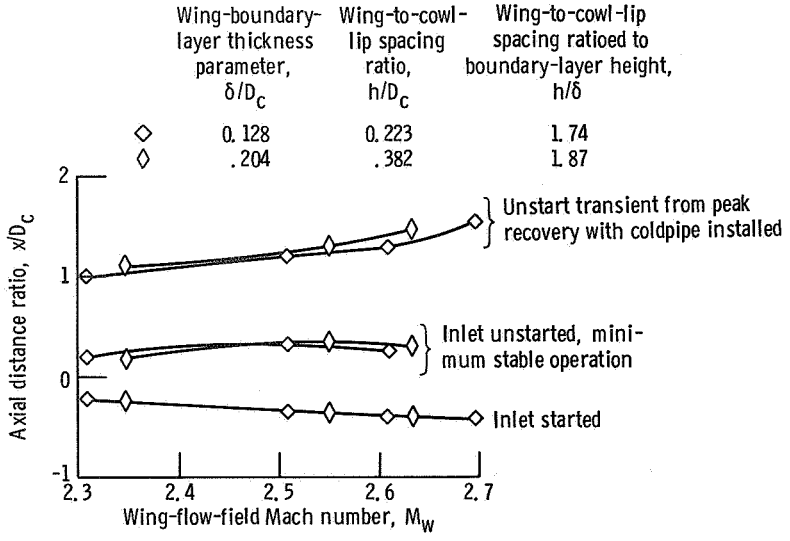


Figure 27. - Forward extent of inlet-shock and wing-boundary-layer interaction with cowl lip about 1.8 boundary-layer heights from wing.

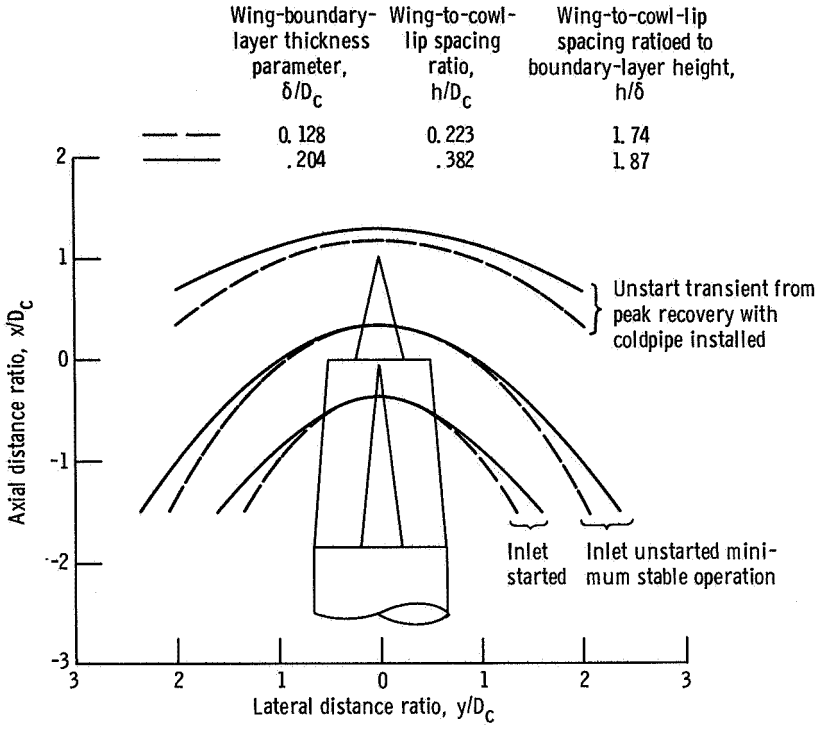


Figure 28. - Effect of boundary-layer thickness on extent of inlet-shock and wing-boundary-layer interaction obtained with cowl lip about 1.8 boundary-layer heights from wing. Nominal wing-flow-field Mach number, $M_w = 2.5$.

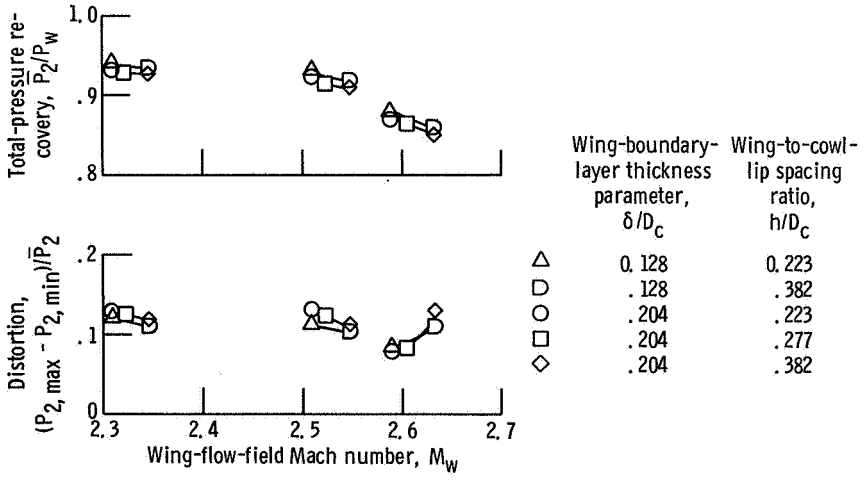


Figure 29. - Critical inlet performance.

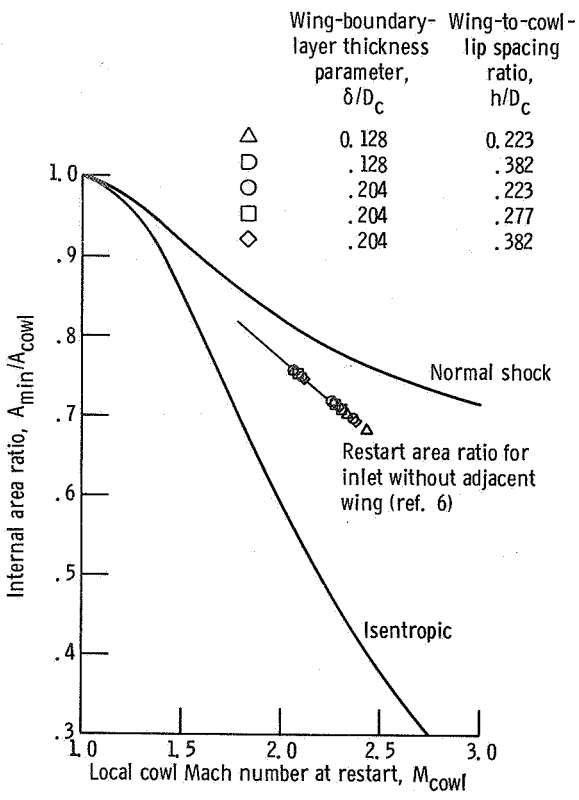


Figure 30. - Effect of wing boundary layer on restart area ratios.

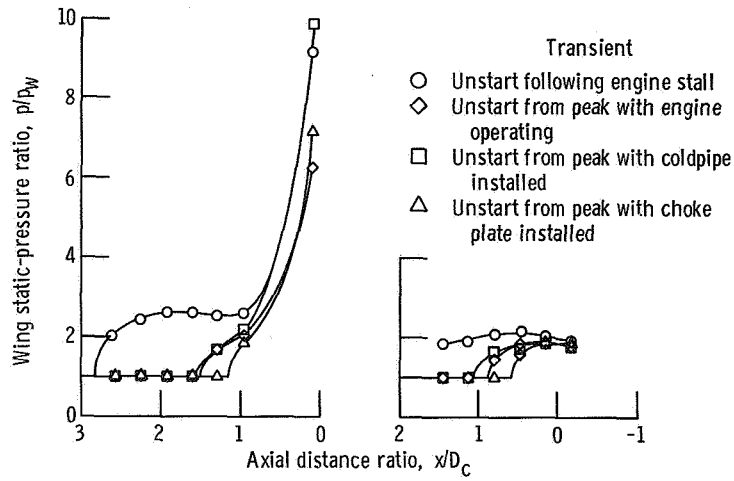


(a) Centerline profile.

(b) Profile at 1.93 $D_c$ from inlet centerline.

Figure 31. - Maximum wing static pressure recorded during inlet unstart transients. Nominal Mach number, 2.5; wing-boundary-layer thickness parameter, $\delta/D_c$ = 0.204; wing-to-cowl-lip spacing ratio, $h/D_c$ = 0.223.

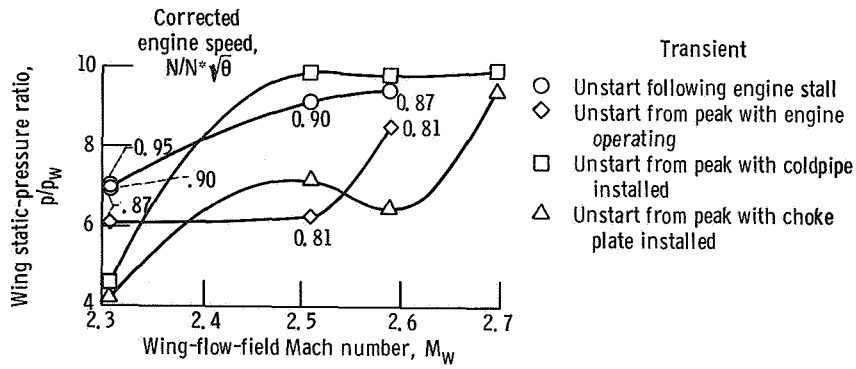


Figure 32. - Maximum wing static pressure measured 0.1 $D_c$ forward of inlet cowl-lip station during unstart transients. Wing-boundary-layer thickness parameter, $\delta/D_c$ = 0.204; wing-to-cowl-lip spacing ratio, $h/D_c$ = 0.223.

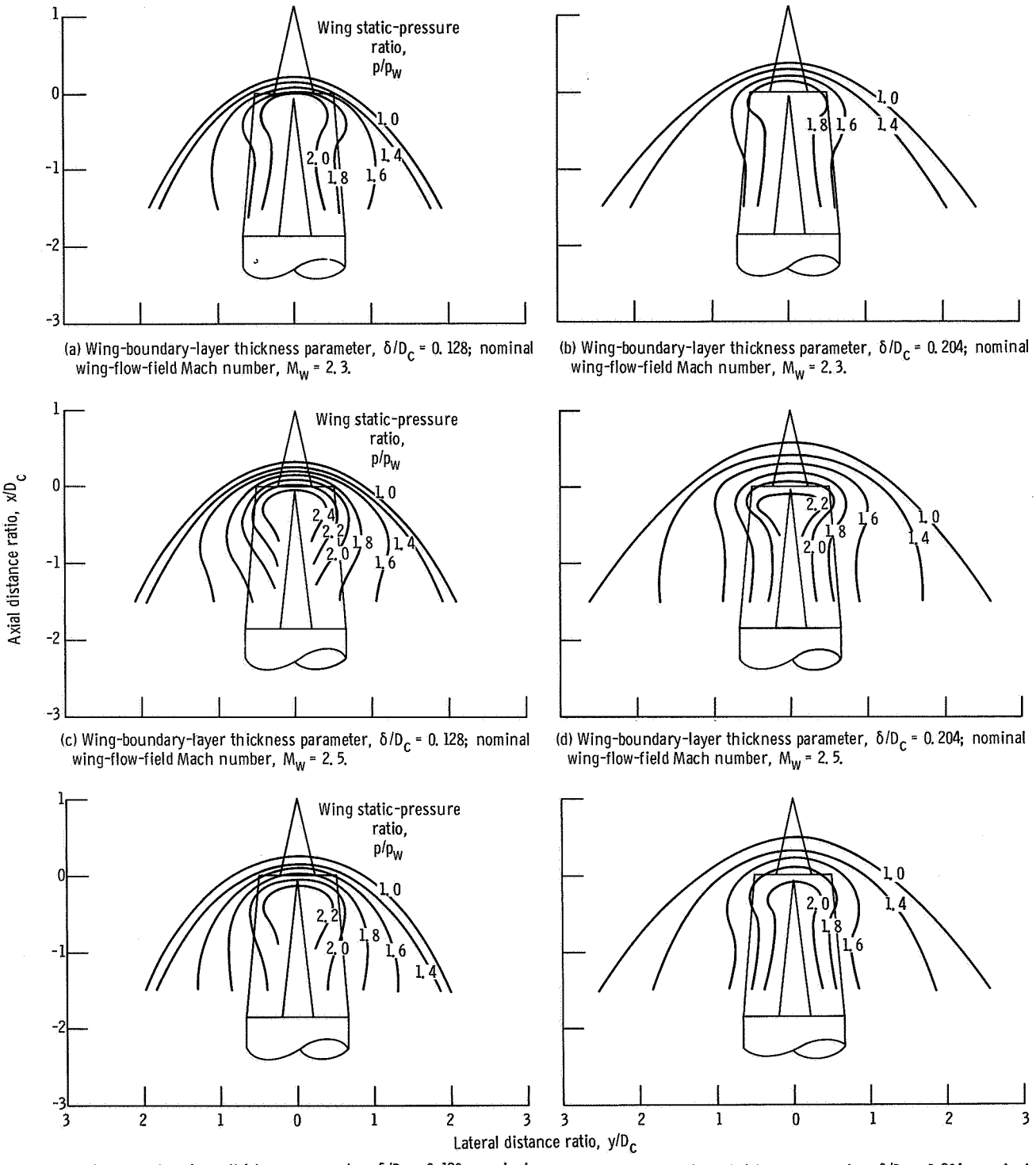


(a) Wing-boundary-layer thickness parameter, $\delta/D_c = 0.128$; nominal wing-flow-field Mach number, $M_w = 2.3$.

(b) Wing-boundary-layer thickness parameter, $\delta/D_c = 0.204$; nominal wing-flow-field Mach number, $M_w = 2.3$.

(c) Wing-boundary-layer thickness parameter, $\delta/D_c = 0.128$; nominal wing-flow-field Mach number, $M_w = 2.5$.

(d) Wing-boundary-layer thickness parameter, $\delta/D_c = 0.204$; nominal wing-flow-field Mach number, $M_w = 2.5$.

(e) Wing-boundary-layer thickness parameter, $\delta/D_c = 0.128$; nominal wing-flow-field Mach number, $M_w = 2.6$.

(f) Wing-boundary-layer thickness parameter, $\delta/D_c = 0.204$; nominal wing-flow-field Mach number, $M_w = 2.6$.

Figure 33. - Wing static-pressure contours with the inlet unstarted and stable. Wing-to-cowl-lip spacing ratio, $h/D_c = 0.223$.



NASA-Langley, 1971 —— 1 E-5983

NATIONAL AERONAUTICS AND SPACE ADMINISTRATION
WASHINGTON, D.C. 20546

OFFICIAL BUSINESS

FIRST CLASS MAIL

POSTAGE AND FEES PAID
NATIONAL AERONAUTICS AN
SPACE ADMINISTRATION

POSTMASTER: If Undeliverable (Section 158
Postal Manual) Do Not Retur

*"The aeronautical and space activities of the United States shall be conducted so as to contribute . . . to the expansion of human knowledge of phenomena in the atmosphere and space. The Administration shall provide for the widest practicable and appropriate dissemination of information concerning its activities and the results thereof."*

—NATIONAL AERONAUTICS AND SPACE ACT OF 1958

# NASA SCIENTIFIC AND TECHNICAL PUBLICATIONS

TECHNICAL REPORTS: Scientific and technical information considered important, complete, and a lasting contribution to existing knowledge.

TECHNICAL NOTES: Information less broad in scope but nevertheless of importance as a contribution to existing knowledge.

TECHNICAL MEMORANDUMS: Information receiving limited distribution because of preliminary data, security classification, or other reasons.

CONTRACTOR REPORTS: Scientific and technical information generated under a NASA contract or grant and considered an important contribution to existing knowledge.

TECHNICAL TRANSLATIONS: Information published in a foreign language considered to merit NASA distribution in English.

SPECIAL PUBLICATIONS: Information derived from or of value to NASA activities. Publications include conference proceedings, monographs, data compilations, handbooks, sourcebooks, and special bibliographies.

TECHNOLOGY UTILIZATION PUBLICATIONS: Information on technology used by NASA that may be of particular interest in commercial and other non-aerospace applications. Publications include Tech Briefs, Technology Utilization Reports and Technology Surveys.

*Details on the availability of these publications may be obtained from:*

SCIENTIFIC AND TECHNICAL INFORMATION OFFICE

NATIONAL AERONAUTICS AND SPACE ADMINISTRATION

Washington, D.C. 20546